QUASI-STATIC AND CREEP BEHAVIOR OF ENHANCED SIC/SIC CERAMIC MATRIX COMPOSITES

VINAYAK PANDEY

Thesis submitted to the faculty of the
Virginia Polytechnic Institute and State University
in partial fulfillment of the requirements for the degree of

Master of Science
in
Engineering Mechanics

Kenneth L. Reifsnider, Chair
Scott W. Case
Stephen L. Kampe

June 19, 2000
Blacksburg, VA

Keywords: Enhanced SiC/SiC, Creep, Recovery, Quasi-Static, Ceramic Matrix Composites, Inelastic Strain, Finite Element Analysis, Plasticity

QUASI-STATIC AND CREEP BEHAVIOR OF ENHANCED SIC/SIC CERAMIC MATRIX COMPOSITES

VINAYAK PANDEY

(ABSTRACT)

Continuous Fiber Reinforced Ceramic Composites (CFCC's) are being currently investigated as potential materials for high temperature applications such as combustor liners in stationary gas turbines. The creep behavior of woven Enhanced SiC/SiC composites was studied at temperatures from 600 to 1200 °C and at 140 to 220 MPa stress levels. Most researchers studying the creep behavior of ceramic matrix composites (CMCs) use the time hardening model and rate equations for expressing the dependence of creep strain on time, temperature and stress. Such laws, although simple and easy to use, are inadequate to represent the creep behavior over a range of stress levels and temperatures and cannot be used to quantify the pest phenomenon commonly observed in CMCs. Hence, these laws were modified to include the pest phenomenon and an empirical equation was developed that can be used to represent the creep behavior at various stresses and temperatures. The modified equation was used in the finite element analysis and the results were compared with the time and strain hardening models. Microscopic observations on the fractured surfaces revealed the pseudo-ductile behavior of the material at high temperatures. A quasi-static test was conducted at 1200 °C to determine the unloading response of the material. The stress-strain response of the composite demonstrates a hysterisis loop and a small amount of permanent strain, which are characteristic of the CMC's [3]. Finally, a test was

conducted at 1200 ^{o}C to investigate the recovery behavior of the material. The material exhibits a tendency to recover the accumulated creep strain as well as the small permanent strain upon unloading, if sufficient time is allowed for recovery.

The creep data were also modeled using the representations such as Monkmon-Grant and Larsen-Miller equations. A modified Monkman-Grant equation was used to model the stratification of the creep strain rate data with temperature. A finite element model based on the plasticity theory was developed to simulate the quasi-static cyclic behavior of the material. Though the loading behavior of CMCs can be modeled using the bilinear or multilinear kinematic hardening plasticity models, the unloading behavior as predicted by the models is entirely different from the experimentally observed behavior. Hence, these models were modified to correctly predict the stress-strain behavior. The model, which was input via a user defined subroutine into the ANSYS finite element program uses the concept of state or internal variables to define the unloading portion of the stress-strain curve. The results were compared with the test data and they show very good agreement. The model was then used to predict the stress-strain response of a plate with a notch. The results from the analysis were compared with the experimental data and they show good agreement if average values of strains are considered.

ACKNOWLEDGEMENTS

First and foremost, I would like to thank my mother for her everlasting encouragement and love. She has been a constant source of inspiration, and has always encouraged and helped me. Without her, I cannot imagine my present life. This work is dedicated to her.

My deepest gratitude goes to my advisor, Professor Ken Reifsnider, for his valuable assistance, guidance and expertise. I commend him for his academic achievement and his affable personality. Working with Prof. Reifsnider has been a great learning experience for me. I thank him for this excellent opportunity to work in this exciting and developing area.

I would like to extend my thanks to Dr. Scott Case, Dr. Stephen Kampe, Mr. Mike Pastor, Dr. Howard Halverson and Mr. Mac McCord, for their tremendous help during the course of my research work.

Also, I would like to thank all the other MRG members who were always there to help whenever I needed it.

And last, but not the least, I am grateful to Shelia Collins for her assistance in my successful completion of this program.

TABLE OF CONTENTS

LIST OF FIGURES

LIST OF TABLES

CHAPTER ONE

1.1. INTRODUCTION

Recent years have seen tremendous growth in the development of new materials that are lighter, stronger, more corrosion resistant, and capable of performing at elevated temperatures. Continuous Fiber Reinforced Ceramic Composites (CFCC's) are being currently developed as materials having these desirable properties. The potential uses for these materials are in the energy, aerospace, and other related industries. Though monolithic ceramics have good compressive strengths, they are very sensitive to defects present in the material due to fabrication and have low fracture toughness. The use of CFCC's offers a possible replacement of monolithic ceramics and a solution to increasing fracture toughness and in-service reliability [4]. The possible industrial applications of these materials include stationary engines, heat recovery equipment, burners, heat exchangers, combustors and furnace internal parts. The CFCC's include a variety of composites such as SiC/SiC, SiC/CAS, SiC/Alumina, SiC/SiNC and oxide/oxide systems. The growing demand for efficient energy generation and the need to reduce environmental effects of power generation (i.e. NOx and CO emissions) has led to the introduction of CFCCs into the energy and power generation industry. Typical applications include combustors, liners, and discrete components like valves, heads, nozzles, glow plugs and vanes for stationary heat engines like diesel and gas turbine engines [4]. The material being investigated in this study is Enhanced SiC/SiC composite which is used in the SiC/SiC CFCC liners in the ceramic stationary gas turbine(CSGT) engines by Solar Turbines Incorporated [5]. These liners have been tested for more than 10000 hours and the CGST engines have functioned normally, co-

generating both electric power and steam. The use of these liners has demonstrated low emissions of NOx and CO consistently [5]. Since these materials are used at high temperatures, oxidation of Si and C is a major problem. The phenomenon of oxidation embrittlement or the “pest behavior” has been reported for a variety of ceramic matrix composites with non-oxide fibers [9]. Hence, the exposed surface of the liners are coated with Environmental Barrier Coatings (EBC’s) which protect the underlying silica-forming ceramic from undergoing oxidation and hence reduce the environmental degradation of these materials in the combustion environments [5]. These materials are currently being fabricated using various techniques such as chemical vapor infiltration (CVI), melt infiltration, DIMOX^{TM}, and polymer impregnation pyrolysis (PIP). Broadly, most SiC/SiC ceramic matrix composites have three main constituents, a fiber, an interface and a matrix. The interface provides fiber-matrix bonding and control the non-brittle behavior of the composite. The most commonly used interface materials are carbon and boron nitride [7].

In the material investigated in the present study, the SiC fiber is an Enhanced Ceramic Grade Nicalon, the interface is carbon and the matrix is SiC. The fiber has a 5-harness satin weave appearance whereby continuous fiber preforms are fabricated by weaving the fibers in a particular pattern. The composite plate preforms are fabricated by stacking layers of satin weave Nicalon^{TM} SiC fabric in an alternating 0/90^{o} pattern. As a result, the composite has about 35 volume percent silicon carbide fibers and the composite exhibits isotropic behavior in plane until the elastic limit [6]. The chemical vapor infiltration technique is used to deposit a carbon coating on the fiber surface. Then the silicon carbide is deposited on the carbon preform using CVI. An “oxygen

getter" is added to the matrix to remove the traces of oxygen from the coating. This material seals any cracks in the material and hence, improves the service life of the composite [6].

1.2. OBJECTIVE OF THE PRESENT STUDY

The objective of the present study is to investigate the quasi-static and creep behavior of Enhanced SiC/SiC composites in air over a range of temperatures and stress levels. To completely study the quasi-static behavior, both the loading and the unloading response have to be studied. Another important property to be observed is the creep/recovery behavior of the material. The final goal is to be able to develop a finite element model that can simulate the behavior of the material. Finally, the model is to be used to predict the stress and strain distribution in a plate with a hole.

The present study is divided into two parts. The first part is the experimental work that involves quasi-static, cyclic, and creep testing of the composite specimens at different temperatures and stresses. The important aspects to be considered in the above test are unloading behavior, pest behavior and recovery behavior of the material.

The second part involves modeling of the test data to obtain parameters that are then used as input into the finite element analysis of the creep behavior. Also, a finite element model is developed to understand the loading-unloading behavior of the material and results from the analysis are compared with the test data. The model is then applied to a non-uniform geometry such as plate with a hole or a notch.

1.6. THESIS OVERVIEW

An introduction to Continuous Fiber Reinforced Ceramic Composites and their applications in industry is provided earlier in this chapter. Some of the important properties of the SiC/SiC composites are also discussed. Also, a brief description of the fabrication aspects of the material used in the study is provided.

The ongoing research and a summary of the work that has been done in this field is described in chapter two. A lot of research has been done on similar materials and an effort is made to understand some of the important aspects of the behavior of CMCs. The issues include hysterisis loop behavior of the stress-strain curve, pest behavior at intermediate temperatures, and recovery.

Chapter three deals with the experimental testing done in order to investigate various properties of the material. A brief study of the fracture surface examination using SEM is also discussed.

Chapter four describes the modeling of the test data and inferences about the material behavior. The finite element technique used in the study is presented and a comparison with the test results is made.

Chapter five deals with the extension of the model to a plate with a notch. The experimental work conducted using a double-notched specimen and the comparison with the finite element results are discussed.

Chapter six gives a brief conclusion and scope for future work in this field.

CHAPTER TWO

2.1. INTRODUCTION

The most promising materials in the ceramic matrix composites (CMC's) category in terms of thermo-mechanical properties are the continuous fiber reinforced ceramic composites(CFCC's) which consist of a continuous ceramic fiber embedded in a ceramic matrix, the most common being SiC/SiC composites. Creep and stress-rupture are two important factors in the design of components for thermo-mechanical applications. All components in service undergo many loading-unloading cycles. Hence, issues like strain-recovery and permanent deformation are also of prime importance and should be studied in detail. This review describes the fabrication aspects, material properties, and response of CMC's to thermal and mechanical loads. Both constant and cyclic loading conditions are discussed. There is an increased effort to model the behavior using finite element method; and a review of the modeling work done is also discussed.

2.1.1. PROCESSING OF CERAMIC MATRIX COMPOSITES

The mechanical behavior of CMC's is greatly influenced by the processing conditions. Further, to increase the toughness of these materials, it is necessary to weaken the fiber-matrix bonding, which is primarily done by adding an interphase material. This results in matrix crack deflection around the fibers and hence the fibers are protected against early failure. CMC's are fabricated by a variety of processes such as isothermal/isobaric chemical vapor infiltration (I-CVI), polymer impregnation and pyrolysis (PIP), slurry impregnation/hot pressing (SMP), and melt infiltration. These

methods involve liquid or gaseous precursors with the fiber preform being the starting material. Common liquid precursors are liquid Al for alumina, liquid Si for SiC, organometallic polymers, sol-gels or slurries. The common gaseous precursors include carbon, SiC, Si_3N_4, BN and refractory oxides such as alumina [32]. CVI involves gas phase routes where the matrix is formed in-situ as the result of chemical reactions involving a gaseous precursor. When the conditions are isothermal/isobaric(I-CVI), the preform densification process is slow but highly flexible. The rate of densification can be greatly improved by applying pressure or a thermal gradient to the preform. For imparting special properties to the matrix or the interphase, sometimes a pressure pulsed CVI(P-CVI) technique is used [19]. The PIP and SMP techniques are modifications of the techniques utilized for polymer matrix composites or/and monolithic ceramics. The melt infiltration is a liquid phase technique where the densification of the preform involves the reaction of the liquid(Al or Si) with the preform or the atmosphere(O_2 or N_2)[19].

Among the SiC/SiC class of CMC's, the most common method of production is by the CVI technique. Suemitsu et al. studied the comparison of the performance of SiC/SiC composites used for ceramic gas turbine components made by CVI with the conventional processing methods [20]. They found that the matrix formed by CVI had twice the residual strength after heat cycle tests. The result was attributed to the formation of the silicon carbide film by CVI that prevented the damage to the ceramic fiber by oxidation. Chemical vapor infiltration (CVI) is simply the chemical vapor deposition on the internal surfaces of a porous preform and is a unique method for

preparing continuous fiber ceramic composites. This process has a major advantage that the fibers are not subjected to severe thermal and mechanical stresses as a result of the densification process [8]. But the process is complex and slow and hence it requires a comprehensive understanding of the chemical kinetics and heat and mass transfer fundamentals. A great deal of study is being conducted on the CVI process in at effort to maximize the rate of matrix deposition and minimize the density gradients [8].

2.1.2 INTERPHASES IN SIC/SIC CERAMIC MATRIX COMPOSITES

The mechanical behavior of SiC/SiC composites is greatly influenced by the bonding between the fiber and the matrix. If the bonding is too strong, the composites tend to be very brittle. Hence, in order to introduce ductility and make them tougher, the bonding is weakened by the addition of a thin layer of interphase material between the matrix and the fiber [7]. The weak interphase leads to some beneficial properties such as deflection of matrix cracks along interfaces allowing intact fibers to bridge matrix-crack faces. Though the use of interphase results in better fracture toughness and increased ductility, the creep and fatigue resistance is affected adversely.

The desired properties of an interphase in a SiC/SiC composite are [7]:

a) load transfer from matrix to fiber

b) ability to deflect the matrix micro-cracks

c) ability to withstand thermal stresses induced during processing

d) chemical compatibililty

All of these properties do not complement each other (e.g. (a) and (b) are contradictory). In the enhanced SiC/SiC composites, glass-forming, boron-based

particulates are added to the matrix that react with oxygen to produce a sealant glass that inhibits the oxidation of the carbon layer [11]. The result is an improvement in the creep and fatigue resistance of the material since at high temperatures, the glass flows into the micro-cracks formed in the matrix and seals them, thus preventing further oxidation [11].

2.2 MATERIAL PROPERTIES

The material used in the present study is a 5 harness satin weave Enhanced Ceramic Grade Nicalon^{TM}/Carbon/SiC composite manufactured by Honeywell Advanced Composites Inc.(formerly Allied Signal Inc.). The physical and mechanical properties for the material are listed in Table 1.1 and 1.2 respectively.

Table 2.1 Physical properties of the Enhanced SiC/SiC composite[6]

PROPERTY	NOMINAL VALUE
Fiber Content	35% by volume
Density	2.3 g/cm^3
Porosity	10% by volume

Table 2.2 Mechanical properties of the Enhanced SiC/SiC composite in air[6]

PROPERTY	UNITS	VALUE	
Tensile		23 ^{o}C	850 ^{o}C
Ultimate Strength	MPa	236	265
Elongation	%	0.47	0.63
Modulus	GPa	125	119
Proportional Limit	MPa	76	82
Compressive			
Ultimate Strength	MPa	577	
Contraction	%	0.43	
Modulus	GPa	141	

2.3 OXIDATION EMBRITTLEMENT (PEST BEHAVIOR)

CMC's are being aggressively pursued as materials to replace super alloys in gas turbines, and higher-powered propulsion systems, which require higher operating temperatures for improved performance. During combustion both Si and C have a tendency to undergo oxidation. This oxidation process is accelerated at high temperatures. Zok et al. [2] have investigated the oxidation phenomenon in the ceramic

matrix composites with non-oxide fibers such as MAS/SiC composite. According to them the oxidation process is predominant at intermediate temperatures (between 500 and 900 °C). Also, the oxidation embrittlement or the “pest behavior” occurs at stresses, which exceed the matrix cracking stress for the composite, and it occurs under both cyclic and constant loading conditions [2]. This behavior is expected because once the matrix has cracked, oxygen can permeate through the material and react locally with fibers and result in further damage of the composite. The oxygen reacts with the fiber coating (generally carbon, or boron nitride) first, resulting in a local debonding between the fiber and the matrix. In the case of SiC fibers, a silicate is formed [10]. This silicate formation results in a local stress concentration around the fiber and diminishes the load carrying capacity of the fiber. This process goes on until the composite is unable to carry any further load and the composite fails [9]. The pest phenomenon is not present at very high temperatures (>1000 °C). This lack of a pesting is due to the fact that at very high temperatures, the silicate becomes viscous and suppresses the oxidation phenomenon by acting as a diffusion barrier [9].Hence, it is important to study the pest behavior of any ceramic matrix composite made of non-oxide fibers. Zok, Evans et al. have designed a test method for identification of the pest temperature for CMC’s [9]. This test is a tensile fatigue test with a temperature gradient over the gage section. Several thermocouples are placed in the gage section to monitor the temperature. The temperature at the failure surface is identified as the pest temperature. Three approaches have been suggested to overcome degradation by oxidation embrittlement:

1. an all oxide composite
2. multiple fiber coatings

3. kinetic retardation through coating and fiber chemistry selection[15].

2.4 QUASI-STATIC BEHAVIOR OF SIC/SIC COMPOSITES

The tensile behavior of the SiC/SiC CMC has been studied by many researchers [12,13]. The monolithic ceramics are linearly elastic to failure, and their strength is dependent upon the largest defect present due to manufacturing. The stress-strain curve of SiC/SiC CMC's exhibits linear behavior up to a proportional limit stress and then the curve is non-linear until failure. The strain at the proportional limit is approximately 30% of the failure strain. The total strain to failure is less than 1% for nearly all types of SiC/SiC CMC's. The non-linearity in the material behavior has been attributed to micro-cracks in the composite as a result of matrix cracking, debonding of the interface between the matrix and the fiber and the resulting interface frictional sliding [12]. The ultimate tensile strength of the Enhanced SiC/SiC is the same as that of a standard SiC/SiC, but the strain to failure is much larger which indicates the fact that the addition of glass-forming particulates in the matrix increases the ductility of the material. Also, the elastic modulus of the Enhanced SiC/SiC composite is much lower than that of the standard SiC/SiC composite [11]. Effinger et al. studied the tensile behavior of the Enhanced SiC/SiC composites over a range of temperatures [13]. They found the modulus of the composite to be constant until 980 °C with a subsequent decrease in value. In addition, they found that the strength of the material increases from room temperature to 650 °C [13]. Also, they mentioned that at very high temperatures (above 1300 °C), the oxidation process of the fiber is predominant and it leads to fiber degradation resulting in loss of fiber strength [13].

2.5 UNLOADING BEHAVIOR IN CERAMIC MATRIX COMPOSITES

A great number of ceramic matrix composites especially those with SiC fibers and a SiC matrices exhibit an interesting behavior during unloading. Zok et al. measured the loading-unloading response of SiC/SiC composites at ambient temperatures [3]. There are two very important characteristics of the stress-strain behavior during unloading. First is that the unloading modulus is much less than the loading modulus and the second is the presence of a small amount of permanent strain upon complete unloading. The reduction in modulus is attributed to matrix cracking [3]. The stress-strain response has been characterized as a hysterisis loop. The area of the hysterisis loop depends on factors such as the type of interface, the applied stress and the number of cycles of loading. The modulus reduction is dependent on the stress level, because as stress increases, there are more cracks in the matrix resulting in a decrease in modulus. Also, the permanent inelastic strain that is accumulated in the material as a result of unloading is less than 5% of the failure strain, which indicates that the behavior of these materials is quite different from monolithic ceramics, or metals that exhibit plasticity. The behavior of the material in compression is linear resulting in hysterisis loops with nearly zero area [22].

2.6 CREEP

At elevated temperatures, creep is one of the most important phenomena affecting the material behavior. Creep is generally defined as the time dependent deformation that occurs when the material is subjected to load for a prolonged period of time. This

phenomenon is greatly accelerated at elevated temperatures especially at temperatures greater than $0.5T^m$ where T^m is the absolute melting point for the material. The most important means of studying the creep behavior of materials so far has been the constant or step load and constant temperature tensile test. Commonly, the data available from such a test are

a) Deformation data, which is usually presented in the form of strain, measured over a gauge length as a function of time. This is called a creep curve.
b) Rupture data, which is the time at which the specimen breaks. Usually rupture curves are plotted as a variation of rupture time with applied stress [21].

The creep curves for most materials show three distinct regions: a primary region with decreasing creep strain rate, a secondary region with constant creep strain rate and Tertiary region with increasing creep strain rate.

Associated with creep are two other phenomena called relaxation and recovery. Relaxation is the reduction in the stress in the material if the strain is held constant. In a relaxation test, the elongation of the tensile specimen is kept constant resulting in relaxation of load. Recovery is the process in which an unloaded material recovers a part or all of the strain accumulated during loading. Figures 2.1 and 2.2 show a typical creep curve and a strain rate curve as a function of time respectively.

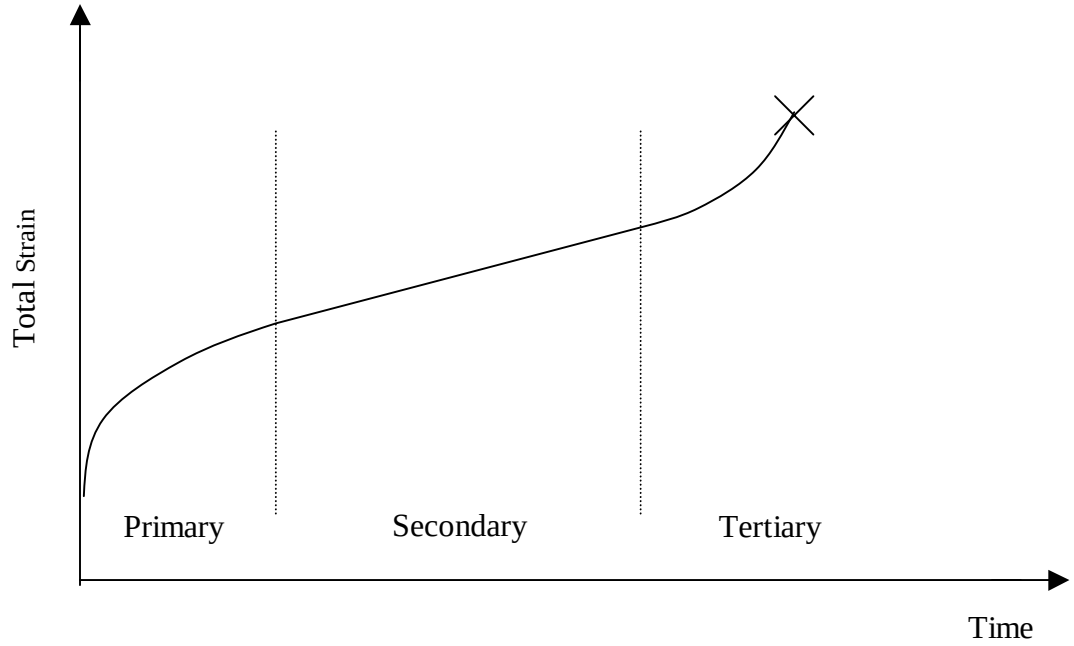

Figure 2.1 – Typical Strain vs time plot during a tensile creep test

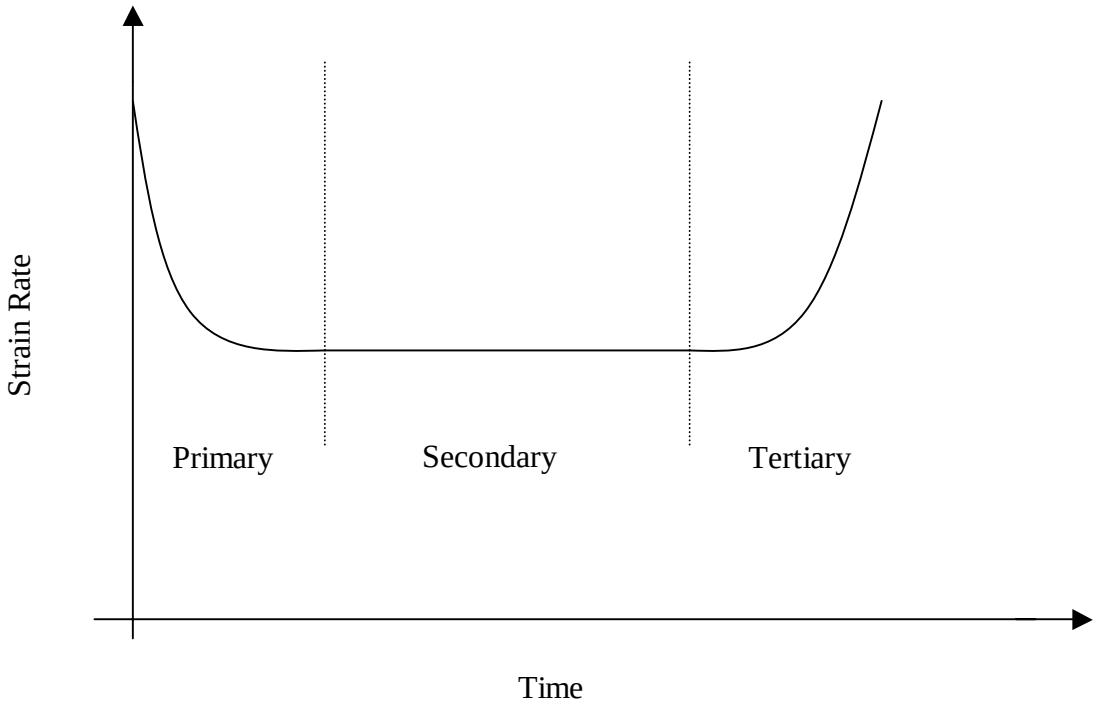

Figure 2.2 -- Typical Strain rate vs time plot during a tensile creep test

2.6.1 CREEP BEHAVIOR OF CMC's

Since CMC's are primarily used in high temperature applications, a great deal of research has been focussed on understanding the creep behavior of these materials. Most of the experimental work conducted on the creep behavior of SiC/SiC composites shows the three regions typically observed in the creep behavior of metals. Zhu et al. [11] have investigated the creep and cyclic creep behavior of Enhanced SiC/SiC composites at 1300 ^{o}C. They assumed the power law equation for the strain rate($\dot{\varepsilon}$) relationship, which is given as

$$\dot{\varepsilon} = A\sigma^{n} \exp\left(-\frac{Q}{RT}\right)$$

where A is a constant, n the stress exponent, Q the activation energy, R the gas constant, and T the absolute temperature. They found out that the stress exponent for static creep is 8 whereas for cyclic creep it is 10 [11]. Cao et al. found out that the stress exponent in the above equation is also dependent on the stress level. They reported that the exponent n could be as low as 1.7 for stresses below 70 MPa and as high as 13.6 for stresses close to 200 MPa [12]. The 70 MPa stress level was identified as the proportional limit stress in the monotonic quasi-static tensile test indicating the importance of matrix cracking in the creep and fatigue behavior of these composites. Lara-Curzio studied the behavior of Enhanced SiC/SiC composites in air at 950 °C. The strain-time curves and the dependence of the loss of strength with time were attributed to the oxidation-induced stress-rupture of reinforcing fiber bundles [18]. The tests results also indicated a continuous increase in the specimen compliance and accelerated deformation or the presence of tertiary region before failure in these CMC's. The study of the fracture surfaces of the failed creep specimens reveals a great deal of information

about the phenomenon. At lower temperatures, there is almost no fiber pullout and there is an indication of brittle behavior[28]. As temperature increases, the fiber pull out also increases and the fracture surfaces show indications of ductile behavior.

2.6.2 CREEP RECOVERY BEHAVIOR OF CMC's

The study of the creep recovery behavior in CMC's and its modeling has received little attention. Most research has been focussed on the recovery of strain upon unloading but it is important to investigate the material behavior after the load is removed and the material is allowed to recover the strain over a period of time. Holmes et. al. investigated the cyclic creep behavior of 0° and 0/90° SiC/CAS, SiC/MLAS and SiC/Si_3N_4 composites at elevated temperatures[34]. Monolithic ceramics exhibit the phenomenon of strain recovery but the amount of recovered strain in CMC's is much higher than in the monolithic ceramics. They introduced two parameters for quantifying the recovery strain behavior.

Figure 2.3 illustrates the approach used by them to study the recovery behavior.

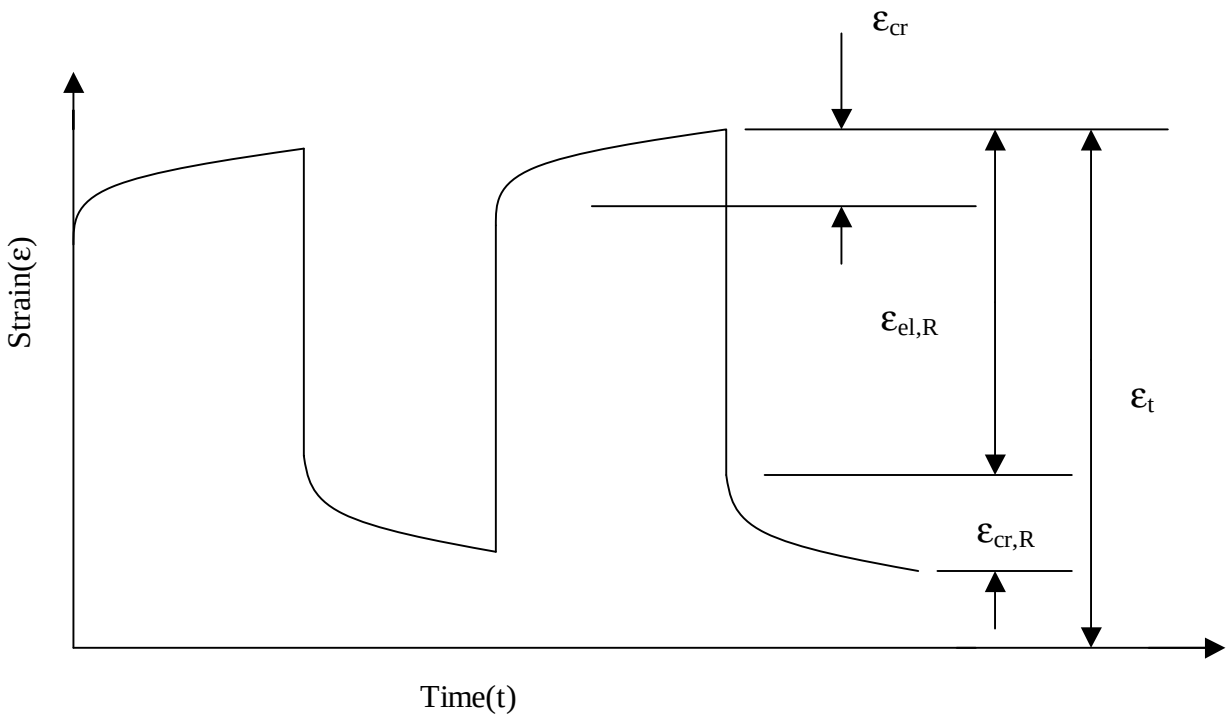

Figure 2.3 – schematic of the terms used in creep recovery[35]

The total-strain recovery ratio R_t is defined as the ratio of the elastic and creep strains recovered in a given cycle to the total accumulated strain present immediately prior to unloading[35].

$$R_t = \left(\varepsilon_{el,R} + \varepsilon_{cr,R}\right) / \varepsilon_t$$

The creep-strain recovery ratio R_{cr} is defined as the ratio of the strain recovered during the unloading portion of a cycle to the creep strain accumulated during the loading portion of the cycle[35].

$$R_{cr} = \varepsilon_{cr,R} / \varepsilon_t$$

It is important to note that the loading and unloading times are to be equal in the previous definitions. For a Nicalon SiC_f/CAS-II composite, R_t is almost 1 at 1273 K and R_{cr} is 27% for 0° composite and 49% for the 0/90° composite [35].

2.6.3 MODELING OF CREEP DATA FROM UNIAXIAL TEST(CONSTANT STRESS)

The stress in the specimen during the uniaxial test is calculated as the applied load divided by the original cross section area and taken to be constant. The deformation in the specimen is dependent on three main parameters: stress, time, and temperature. The creep strain is generally defined as:

$$\varepsilon_c = f(\sigma, t, T)$$

where

ε_c is the creep strain

σ is the applied stress

t is the time

and T is the absolute temperature.

Depending on the material data, usually an approximation to the above relationship is made which can be expressed as

$$\varepsilon_c = f_1(\sigma).f_2(t).f_3(T)$$

The functions for stress, time and temperature have been expressed by a large number of researchers investigating the creep behavior of the materials and in most cases, the functions are proposed to empirically fit the test data.

The use of a separate function for stress is generally related to the secondary creep region of the creep curves. The separation of time and temperature is not as commonly observed as the stress; and generally researchers tend to combine the two effects into one parameter.

The most common forms for the stress function are[21]:

Norton	$f_1(\sigma) = K.\sigma^n$
Soderberg	$f_1(\sigma) = B\{\exp(\sigma / \sigma_0) - 1\}$
McVetty	$f_1(\sigma) = A\sinh(\sigma / \sigma_0)$
Dorn(High Stress)	$f_1(\sigma) = C\exp(\sigma / \sigma_0)$
Johnson, Handerson, and Kahn	$f_1(\sigma) = D_1\sigma^{m_1} + D_2\sigma^{m_2}$
Garofalo	$f_1(\sigma) = A\{\sinh(\sigma / \sigma_0)\}^m$
Hooke-Norton	$\dot{\varepsilon} = \frac{\dot{\sigma}}{E} + K\sigma^n$

The most commonly used function is the power law proposed by Norton because of its simplicity. Dorn [23] has suggested that at low stresses, the power law gives a better fit to the data whereas at higher stress an exponential function is more likely to give an accurate result. Some other workers (e.g. Garofalo [24]) in this field have also proposed that a drastic change in the mechanism is unlikely when one goes from a lower stress to a higher stress and hence he suggested a combination of power law and the hyperbolic sine law as shown above.

The time dependence on creep behavior has been investigated in great detail. Hence, the number of expressions proposed is very large. Most of the expressions involve a sufficient number of arbitrary constants and a combination of several functions. For a

material which undergoes drastic changes in microstructure with time at high temperatures, the task of finding a function that accurately describes the time dependence of creep is very difficult except by extensive curve fitting procedures [21]. The empirical approach that is widely used by engineers, may not give correct results when dealing with variable-stress creep. Another approach is to separate the time dependence into parts and associate a physical behavior with each term.

Nevertheless, the empirical approach is widely used especially in conjunction with the finite element method. Some of the expressions commonly used are [21]:

Andrade	$f_2(t) = (1 + bt^{1/3}) \exp(kt) - 1$
Bailey	$f_2(t) = Ft^n$
McVerty	$f_2(t) = G(1 - e^{-qt}) + Ht$
Graham and Walles	$f_2(t) = \sum a_i t^{n_i}$
Secondary Creep	$f_2(t) = kt$

The effect of temperature on creep strain is twofold. First, the material constants change with temperature. This implies that the functions of stress and time may have constants that vary with temperature. In order to account for the variation, one has to take into account the range of temperature experienced by the material and then fit the temperature function and at the same time adjust the values of constants appropriately. Secondly, the microstructure of the material may also change with temperature. A slip process dictates creep in metals at temperatures below $0.4T^m$ where T^m is the absolute melting temperature. The rate of creep strain continually decreases due to strain hardening as dislocations encounter obstacles and tend to immobilize [21]. As the

temperature goes higher, the phenomenon changes to temperature induced diffusion and at temperatures $0.8T^m$ and above, the creep occurs by pure diffusion.

The most common expression for the temperature dependence of creep is the well-known Arrhenius rate equation. This equation is given as

$$f_3(T) = \exp(-Q / RT)$$

Dorn[23] found that if creep strain is plotted as a function of the parameter

$$t \exp(-Q / RT)$$

then the creep data at different temperatures may be plotted on a single curve. He suggested the creep law in the following form

$$\varepsilon_c = f\{t \exp(-Q / RT)\} f_1(\sigma)$$

which can be extended to a more generalized form such as

$$\varepsilon_c = f\{t \exp(-Q / RT)\}^n f_1(\sigma)$$

An important aspect of the curve fitting procedures for creep data is that the laws that give satisfactory results under constant stress conditions might not be applicable under variable stress conditions. For instance, a creep law of the form

$$\frac{d\varepsilon_c}{dt} = g(\sigma, \varepsilon, t, etc.)\, f_3(T)$$

cannot be used for a variable stress condition just by taking the time derivative though it might be acceptable for constant stress condition[21].

Some other temperature functions used in the past are

Boyle, Spence $\varepsilon_c = C \exp(-Q / RT) t^m \sigma^n$

Kauzmann $\dot{\varepsilon}_c = A \exp\left(-\frac{Q - \gamma\sigma}{RT}\right)$

Lifszic $$\dot{\varepsilon}_c = \frac{\sigma}{T}\exp(-Q/RT)$$

2.6.4 MODELING OF CREEP AT VARYING STRESS

TIME HARDENING MODEL:

This time hardening model states that the creep strain rate is a function of time, stress and temperature [21].

$$\Phi\left(\dot{\varepsilon}_c, \sigma, t; T\right) = 0$$

where Φ is a function

Or

$$\dot{\varepsilon}_c = f_1(\sigma) f_2(t) f_3(T)$$

The time hardening model can be used to model the decreasing creep strain rate during the primary creep phase.

STRAIN HARDENING MODEL:

This model assumes a relationship between the creep strain rate, the accumulated creep strain, the stress and the temperature[21].

$$\Phi\left(\dot{\varepsilon}_c, \sigma, \varepsilon; T\right) = 0$$

ROBTONOV'S THEORY[29]:

This theory is a generalization of the integral form for linear viscoelasticity. The integral representation of creep is given as

$$E(t)\Phi[\varepsilon(t)] = \sigma(t) + \int_0^t K(t-\tau)\sigma(\tau)d\tau$$

where

$K(t-\tau)$ is a function that characterizes the material properties.

This type of relationship implies that the entire history of stress affects the strain response of the material at a given time t.

2.6.5 MODELING THE CREEP DATA FOR CMCs

There are a number of approaches used to characterize and model the creep and creep rupture behavior of ceramic matrix composites, which range from microstructure studies to analyses of strain rates and rupture time. The creep curves for the SiC/SiC composites are similar to the normal creep curves for metals. Zhu et al. [25] have proposed a threshold stress approach to interpret the experimental data for these materials. They have used the power law for curve fitting the strain-time histories obtained from experimental testing. They suggested that the presence of primary, secondary, and tertiary regions of the creep curves is highly dependent on the stress and temperature conditions.

They identified the relationship between the minimum steady state creep strain rate ($\dot{\varepsilon}_m$) as

$$\dot{\varepsilon}_m = A.\sigma^n.\exp(-Q/RT)$$

The stress exponent was found to vary with stress. They also mentioned that there exists a threshold stress level at a given temperature below which the creep strain rate falls below the detectable level[25]. The apparent threshold for SiC/SiC composites measured by them is 75 MPa at 1000 and 1100 ^{o}C, 60 MPa at 1200 ^{o}C and 30 MPa at

1300 ^{o}C. They modified the minimum strain rate equation to include the threshold stress as

$$\dot{\varepsilon}_m = A.(\sigma - \sigma_{th})^n . \exp(-Q'/RT)$$

and found that the data points could be well fitted by a straight line of slope 5 [25]. Although the power law provides a simple and easy method of characterizing the creep behavior of these materials at a given temperature, it has not been used with much success to characterize the creep behavior over a range of temperatures.

The creep rupture time data is generally plotted as a function of stress. This data can be fitted to an empirical equation of the form

$$t_r = B.\sigma^{-N}$$

where t_r is the time to rupture

B is a constant

and N is the stress exponent for stress rupture.

A typical value of N for CMC's is 5.8 at 1000 °C[25] and it is found to vary with temperature.

The steady-state creep strain rate data is generally plotted against time to rupture and the curve fit to the data is given most often by the Monkman-Grant Relationship [26].

The relationship is defined as

$$t_r . \dot{\varepsilon}^m = C_{M-G}$$

where

m is the strain rate exponent

and C_{M_G} is a material constant.

The Larsen-Miller parameter(P) is one of the most widely used methods for predicting the creep life of materials esp. metals. The expression for the parameter is given as

$$P = T.(C + \log t_r)$$

The constant C for SiC/SiC composites is found to vary between 5-10[25].

2.7 FINITE ELEMENT ANALYSIS OF CREEP BEHAVIOR

The formulation of the finite element problem for analysis of creep behavior starts with the virtual work expression[30].

$$\int_v \varepsilon^T \sigma dV - \int_v u^T b dV - \int_s u^T p dS = 0$$

where b is the body force vector, p is the surface traction vector and

$$\varepsilon = [L]u$$

[L] is the matrix operator containing the compatibility conditions.

u is the displacement vector and ε is the strain vector.

The total strain is decomposed into an elastic(ε_E) and creep(ε_c) component.

$$\varepsilon = \varepsilon_E + \varepsilon_c$$

The elastic stress-strain relation gives the elastic component of the strain

$$\sigma = [D]\varepsilon_E$$

The unknown components u are expressed in terms of shape functions for an element as

$$u = [N]a$$

where a is the vector of unknown constants to be determined.

Using the weak form approach, the following algebraic equation results

$$[K]a - F_c - F = 0$$

where

K is the stiffness matrix

F is the force vector

and F_C is the creep force vector given by

$$F_c = \int_V [B]^T [D] \varepsilon_c dV$$

and

$$[B] = [L][N]$$

ε_c is usually given in the following form

$$\varepsilon_c = f(\sigma, t)$$

Using the above constitutive relation for creep strain, the problem can be formulated as an initial value problem with stress as unknowns.

where

$$\frac{d(\sigma - \sigma^0)}{dt} = [D][B][K]^{-1}(\int_V [B]^T [D] f(\sigma, t) dV) - [D] f(\sigma, t)$$

$$\sigma^0 = [D][B][K]^{-1} F$$

and the initial condition is given as

$$\sigma(0) = \sigma^0(0)$$

The above equation can be solved using an explicit or implicit Euler algorithm. Holmes and Park [33] developed a two and three dimensional finite element model for fiber reinforced ceramics where the fiber packing can be approximated by a hexagonal or rectangular array. They postulated that the overall mechanical behavior of the composite structure can be modeled by use of a geometric unit cell. They used the simple power law for the creep strain rate equation. But in woven ceramic composites, it is difficult to identify a unit cell structure. Also, the woven structure gives rise to isotropic properties in a plane so that for 2-D problems, the composite can be approximated by a continuous media with overall isotropic properties such as elastic modulus and Poisson's ratio.

Most CMC's exhibit nonlinear stress strain curves with hysterisis behavior upon unloading. Leckie et al. [42] have modeled such material behavior using damage mechanics concepts. The non-linear loading portion of the stress-strain curve can be modeled using concepts from plasticity such as multi linear kinematic or isotropic hardening, but the unloading behavior is then drastically different from the experimental behavior. One of the goals of the present study is to modify the plasticity laws in order to incorporate the unloading behavior of the material. The main goal is to model the modulus of the material during unloading.

CHAPTER THREE

3.1. INTRODUCTION

The primary purpose of the current experimental work was to obtain the quasi-static and creep properties of the Enhanced SiC/SiC composite over a range of temperatures. Uniaxial tests were performed in order to understand the material behavior as a function of time, stress and temperature. The quasi-static, creep, quasi-static cyclic and creep recovery behavior were investigated. Also, the fracture surfaces of the failed specimens were examined using SEM to observe the effect of test conditions on the microscopic structure of the material and relate to the macroscopic behavior.

3.2. MATERIAL AND SPECIMEN GEOMETRY

The test specimens were made of SiC fiber(Nicalon^{TM}) reinforced Enhanced SiC matrix composite. The weave pattern of the fibers was a five-harness satin weave. The material was fabricated by an isothermal chemical vapor deposition (ICVI) technique and manufactured by Honeywell Advanced Composites Inc. (formerly Allied Signal Inc.). Typically, fiber reinforced composite plate preforms were made by stacking layers of satin weave Nicalon^{TM} SiC fabric in an alternating 0/90° lay-up. The resulting fiber reinforced composite typically contained 35 percent silicon carbide, which exhibits isotropic behavior in plane. A coating of carbon was deposited on the fibers via chemical vapor infiltration (CVI). Carbon acts as a debond layer between the fiber and the matrix. The carbon-coated preform was densified with a silicon carbide matrix via CVI. An “oxygen getter” was added to the matrix to scavenge oxygen away from the coating. This material effectively seals any cracks in the material, thereby increasing its

use life[6]. The specimens, which were dog bone shaped, were grouped into two different thicknesses. One set of 15 specimens with a thickness of 2.5 mm and the other set of 10 specimens with a thickness of 3.5 mm. The specimens with different thickness were tested at the same conditions and no noticeable dependence on the thickness was observed. All the specimens were 200 mm long and 10 mm wide near the grip section. The gage section was 40 mm long and 8 mm wide. The thickness and width of the specimen represent the average values, which were taken by measuring the values at three points within the gage section and then taking the mean of the values. The material exhibits a lot of porosity and variations in the surface that can be observed visually. Figure 3.2 shows the specimen geometry.

3.3. EXPERIMENTAL SETUP

The testing system was comprised of a hydraulic testing frame, a furnace for maintaining high temperature around the specimen, cooling system to remove heat effectively, a high temperature extensometer for measuring the strains and a data acquisition system. The test system is shown in figure 1. An MTS 880 servo hydraulic test frame was used for testing the specimens. The frame was attached to an MTS 458 controller that can be used to program the loading cycle. The load-capacity of the frame was 20,000 lbs. The specimens were loaded quasi-statically in load control at the rate of 10-15 MPa/sec, and the total loading time was less than 15 seconds for all the tests. The tests were all load controlled. The alignment of the load frame had been checked and maintained periodically. The load frame has two sets of water-cooled hydraulic wedge grips for gripping the specimen. The grip pressure was varied between 200-600

psi and it was found that grip pressures higher than 500 psi resulted in failure of specimens near the grips. In the first set of tests, the specimens were tabbed at the end with thin aluminum sheet, which resulted in failure of the specimen at the grips during loading. Subsequently, the tabs were changed to sand paper tabs whereby three layers of coarse grit sandpaper were placed around the specimen ends and secured by means of masking tape. The specimen was then aligned with the grips using a spirit level and finally gripped in the test frame at an appropriate grip pressure. The grip pressure had to be varied because at high loads the specimen had a tendency to slip out of the grips and increasing the grip pressure resulted in failure of specimen at the grips. Hence, by trial and error, a suitable grip pressure for a certain load level was determined. The length of the specimen that was tabbed had to be kept below 1.5 in. because of the limitations on the size of the furnace and the requirements for proper insulation around the furnace. Cooling of the system was achieved by circulating cold tap water through the hydraulic wedge grips, the extensometer and the fixture for holding the extensometer.

A convection/radiation heating method was used to build and maintain high temperature in and around the specimen. The system consists of a clam shell type furnace with four silicon carbide resistance elements. The shell of the furnace was made of stainless steel and the outer dimensions of the furnace were 3.5” high x 3” x 3”[22]. The inside of the furnace was lined with fused silica insulation approximately 0.5” thick. The operation of the furnace was controlled by a microprocessor-based temperature and process controller (master and slave type) [22]. The specimen temperature was monitored by two R-type thermocouples touching the face of the specimen. For optimum temperature

control, the master controller was connected to the thermocouple closest to the top heating element and the slave controller to the thermocouple closest to the bottom heating element[22]. According to the standards of testing for CMC's [43], the target temperature should be reached by monotonically increasing the specimen temperature within about 20 minutes. In order to achieve this rate, the temperature was increased as the rate of 90 °F per minute. The heating rate was greatly influenced by the quality of insulation around the furnace. The furnace was insulated completely from outside by about 0.5" thick insulation pads made of alumina fabric. Once the target temperature was reached, the specimens were soaked at the given temperature for about 20 minutes to stabilize the specimen temperature [22]. The temperature of the specimen was monitored throughout the test by readings from the two thermocouples, which were placed about half an inch apart within the gage section. High temperature strain measurements were made via a one inch gage length extensometer(MTS model 621-51E). The maximum temperature capability of the extensometer was 2200 °F and the calibrated range was 15%. The extensometer was a water-cooled unit, which measured the strain by the deflection of two 5" alumina rods. The rods go through the two holes in the furnace and contact the specimen on the thickness side. The alumina rods were loaded by leaf springs mounted on the heat shield bracket [22]. The ends of the rods were knife edged to aid in mounting the extensometer on the specimen. The extensometer attachment, the heat shield, and the furnace were attached as one unit to one of the posts of the test frame. The data acquisition system was linked to a personal computer for reading the data from the controller.

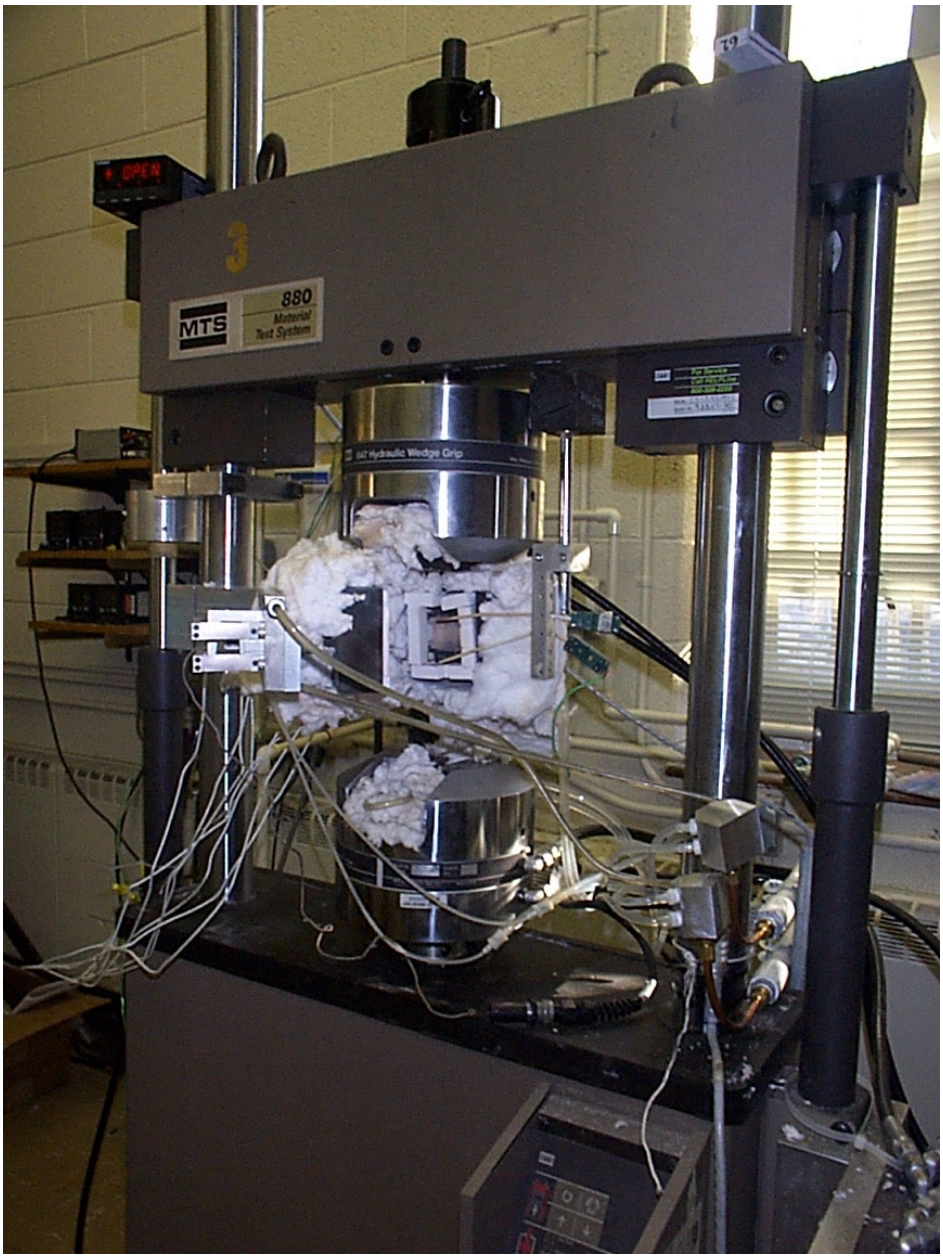

Figure 3.1—Experimental Setup for high temperature testing

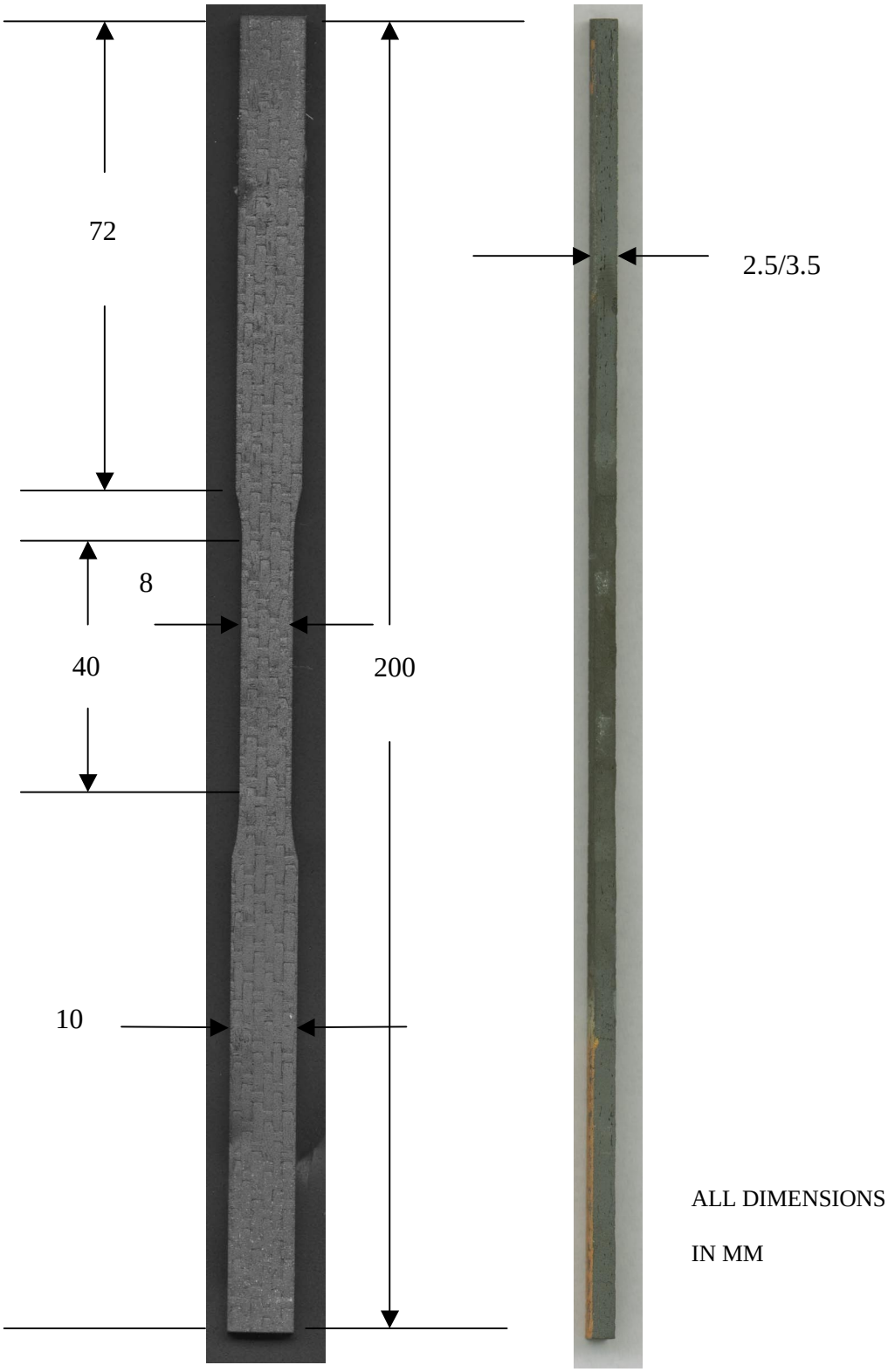

Figure 3.2— Test specimen geometry used in the testing

3.4 DESCRIPTION OF THE TEST MATRIX

The goal of the study was to observe the material behavior over a range of stress levels and temperatures. For creep experiments, a threshold stress level at a given temperature exists below which there is no noticeable creep observed [36]. Hence, the tests were performed at stress levels greater than 140 MPa. The specimens were tested at three different temperatures 600 °C, 825 °C and 1200 °C. The intermediate temperature was chosen to investigate the pest behavior of the material. The cyclic and creep recovery tests were performed at 1200 °C.

3.5 QUASI STATIC BEHAVIOROF ENHANCED SIC/SIC CMCS

Figure 3.3 shows the quasi-static tensile behavior of the material at three different temperatures. The data was obtained from the loading data for creep tests where the specimens were ramped up to a given load level and hence, the loading curve can be used to represent the quasi-static behavior. The prime reason for not doing quasi-static tests was the limitations on the number of specimens. The stress-strain curve exhibits linear behavior until a stress of about 60 MPa and then is non-linear beyond 60 MPa. The initial modulus of the material as measured from the tests was found to vary from 117 MPa to 148 MPa and no obvious dependence on temperature was observed. The proportional limit determined by the 0.005% offset yield strength method as specified by the manufacturer varied from 60 to 80 MPa. The method of determining the proportional limit is shown in Figure 3.4. The proportional limit in case of composites is generally the matrix cracking stress. These values agree closely with the data supplied by the manufacturer. Also, the stress-strain curves were not found to vary significantly with

temperature. Figure 3.3 shows the two extreme stress-strain curves for each temperature and they overlap each other. Hence, it can be inferred that the quasi-static behavior of the material is not greatly influenced by the temperature particularly below the proportional limit.

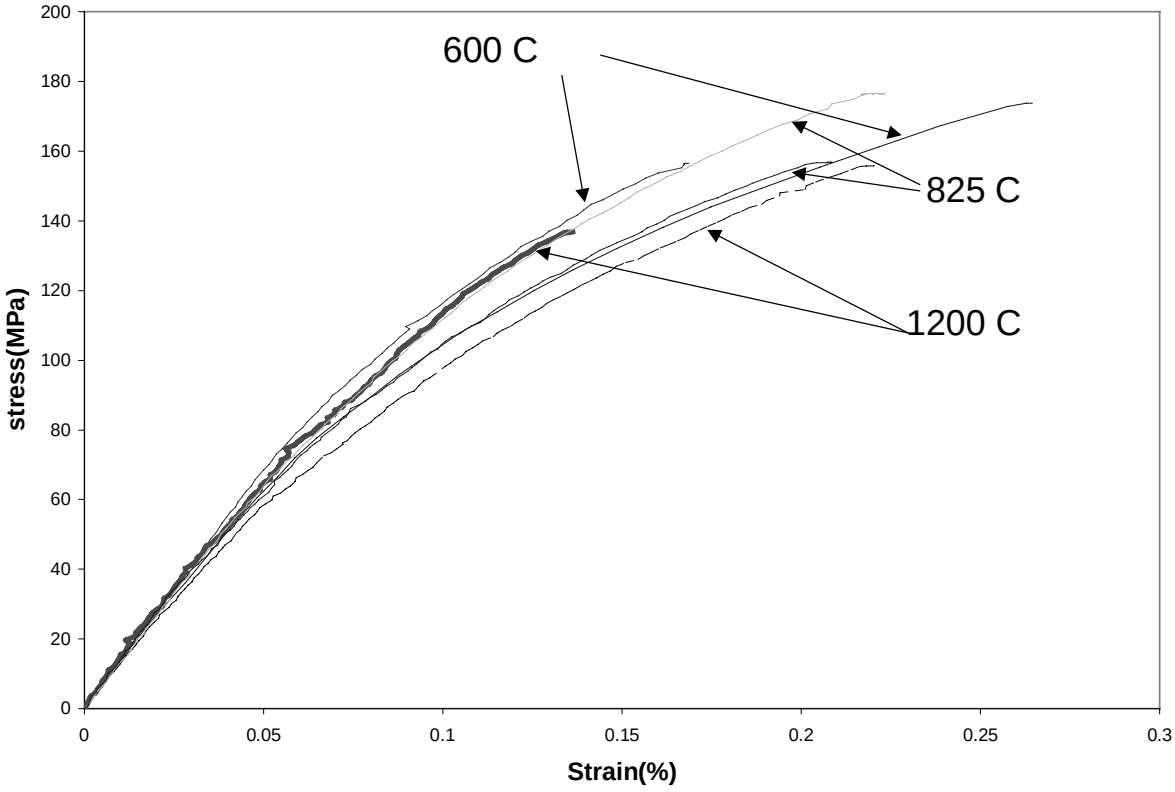

Figure 3.3— Quasi-static behavior of Enhanced SiC/SiC CMC at three temperatures

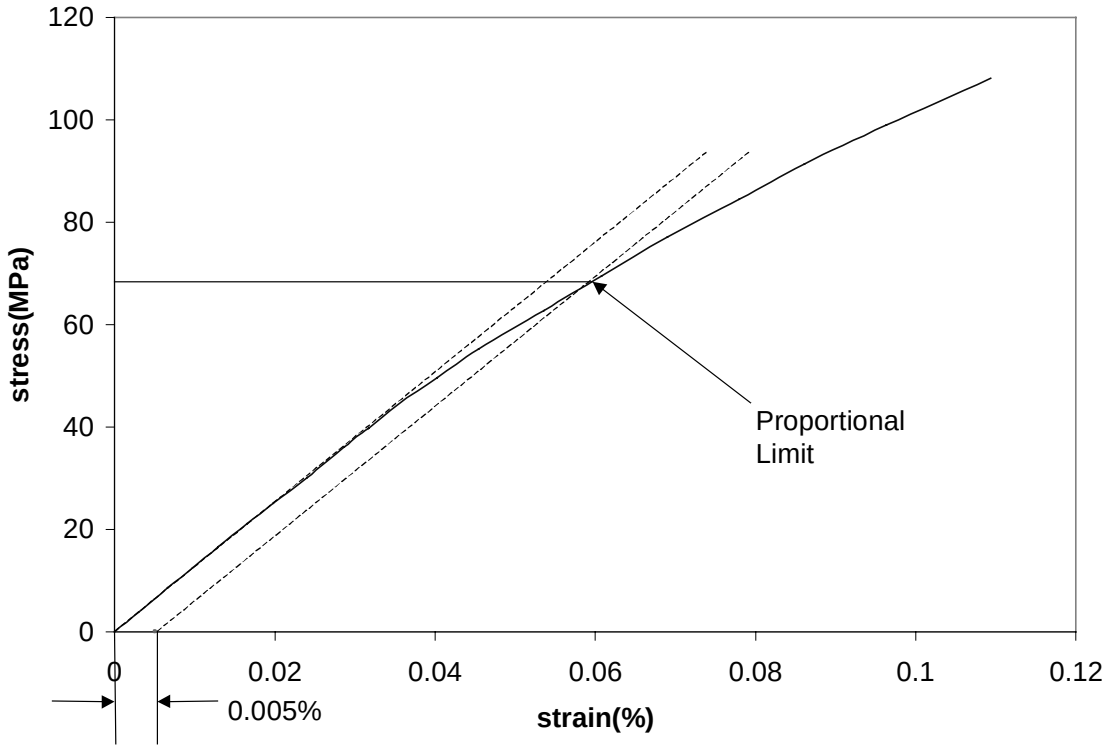

Figure 3.4— Determination of proportional limit for Enhanced SiC/SiC composite

3.6. CREEP BEHAVIOR OF ENHANCED SIC/SIC CMCS

Creep tests were run at three temperatures in order to determine to the creep behavior of the material over a range of temperatures. The CSGT engine operates at an inlet temperature of 1010 °C[6]. Hence the upper limit of the temperature was chosen to be 1200 °C. The other two temperatures were 600 and 825 °C. The 825 °C temperature was chosen because CMCs show a pest phenomenon in the temperature range of 700 to 850 °C. At 600 °C, the stress levels chosen were 160, 180, 200 and 220 MPa. At 825 °C, the stress levels were 140, 160 and 180 MPa. At 1200 °C, the stress levels were 140, 160 and 180 MPa. These stress levels were chosen because the rupture time for these combinations of temperature and stress was less than 100 hours, which is suitable for laboratory testing. Also, Zhu et al. have reported the existence of a threshold stress level for SiC/SiC composites below which there is no creep strain observed [25]. According to them, the threshold stress at 1200 °C is 60 MPa and is 75 MPa at 1000 °C. The tests were repeated to check the repeatability of the creep curves. Though the repeatability in the creep curves was fairly good, the composite showed a variation of an order of magnitude in the rupture times. Not all the tests could be repeated due to the limitation on the specimens. Table 3.1 shows the test matrix along with the rupture time and failure strain for each test. All of the tests were run until the specimen failed due to creep except the test at 140 MPa and 825 °C, which did not fail after 140 hours. Figure 3.5 shows the creep curves for different stresses at 600 °C. The curves exhibit a primary region and secondary region with no tertiary creep that suggests brittle fracture at lower temperatures. The total strain to failure was found to increase with stress except for the 220 MPa stress level whereas the creep strain was

constant and about 0.1%. Figure 3.6 shows the creep curves for different stress levels at 825 °C. The curves exhibit a distinct primary region after which the secondary region is almost flat and after a certain strain, there is a continuously accelerating strain rate region before failure. The minimum secondary creep rates for 160 and 180 MPa curves at 825 °C were found to be lower as compared to those at 600 °C. Also, the strain to failure was lesser than at 600 °C. These data seem to support the theory of pest behavior (oxidation embrittlement) for SiC/SiC composites at intermediate temperatures. A similar trend in the rupture data was not observed. Figure 3.7 shows the creep curves for different stress levels at 1200 °C. These curves show all the three distinct regions of creep. The strain to failure at 1200 °C is almost double the failure strain at 600 °C, which indicates the tendency towards ductile behavior at high temperatures.

Table 3.1 – Test Matrix and rupture data for enhanced SiC/SiC composite at elevated temperatures

Specimen Number	Temperature (^{o}C)	Stress Level (MPa)	Rupture Time (hours)	Strain at failure (%)
0531-21-018-01-05	600	220	0.134	0.3729
0531-21-018-02-05	600	180	13.264	0.2340
0531-21-018-03-05	1200	160	6.058	0.7719
0531-21-018-05-05	1200	180	0.55	0.5941
0531-21-018-06-05	1200	140	4.313	0.7791
0531-21-018-07-05	600	180	5.126	0.3313
0531-21-018-08-05	825	180	1.023	0.2998
0531-21-018-11-05	825	160	69.65	0.3552
0531-21-018-12-05	1200	180	0.534	0.5791
0531-21-018-13-05	825	160	8.261	0.292
0531-21-018-14-05	825	140	140+	did not break
0531-31-018-02-05	600	200	9.98	0.4129
0531-31-018-04-05	600	180	13.64	0.393
0531-31-018-06-05	1200	160	1.34	0.6537
0531-31-018-08-05	600	160	39.598	0.2763
0531-31-018-09-05	1200	140	14.27	0.6115
0531-31-018-10-05	1200	160	4.34	0.7792

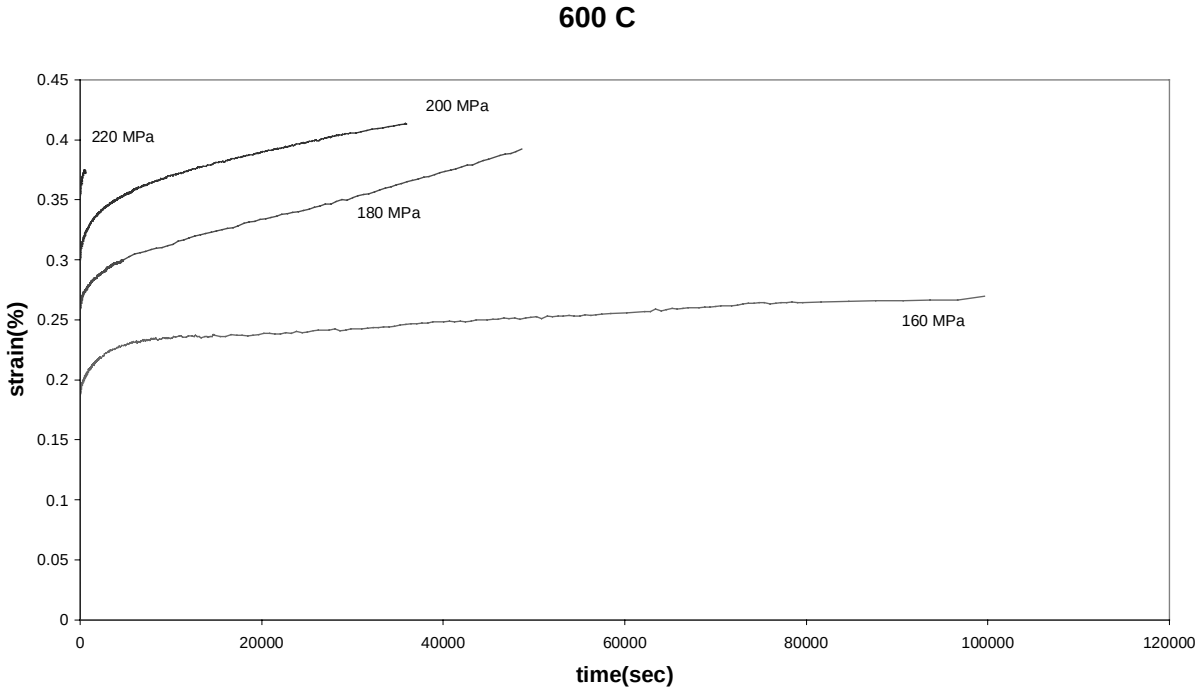

Figure 3.5— Strain vs time plots for different stress levels at 600 °C

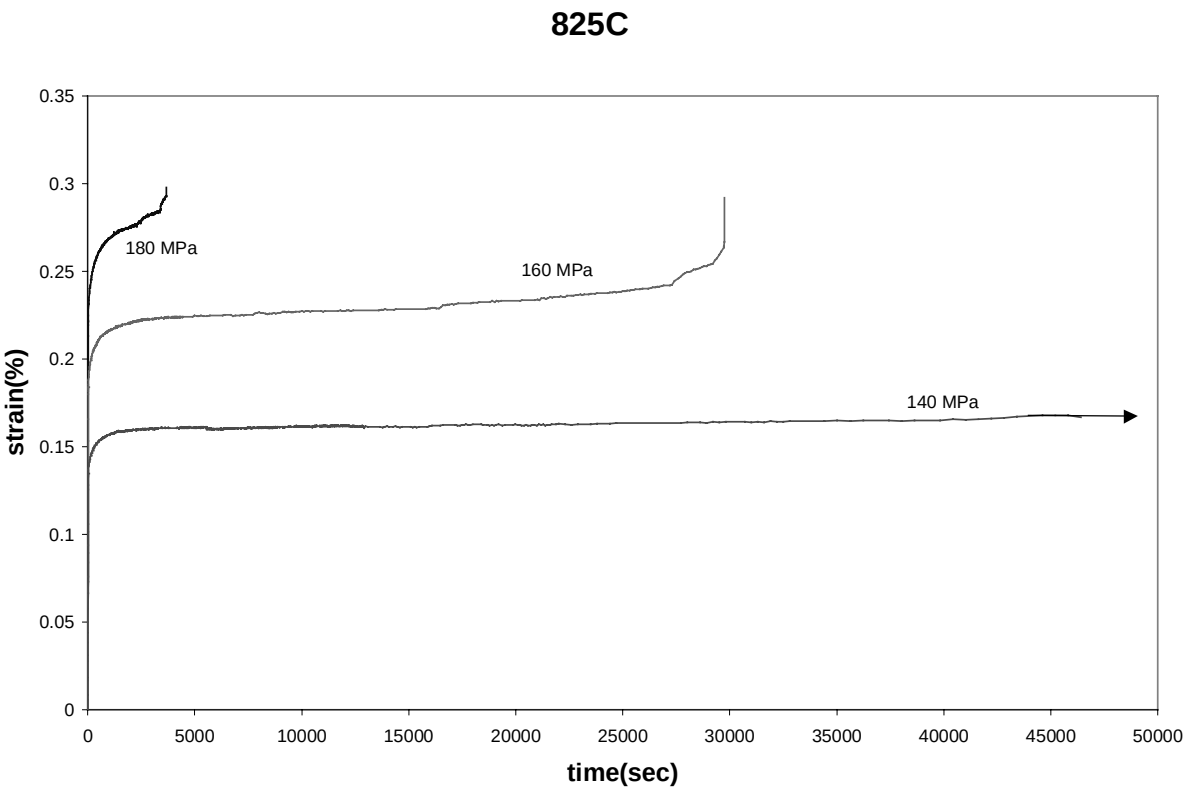

Figure 3.6— Strain vs time plots for different stress levels at 825 °C

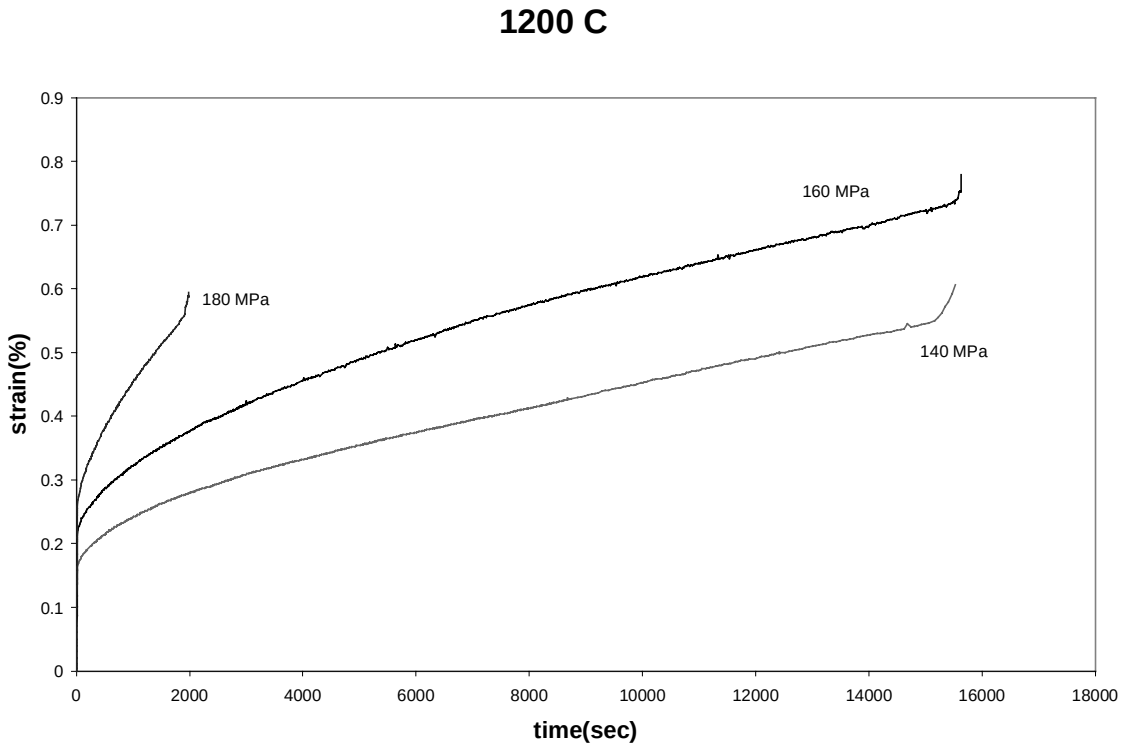

Figure 3.7— Strain vs time plots for different stress levels at 1200 ^{0}C

3.6. MICROSTRUCTURE ANALYSIS

Three different creep specimens, one at each temperature, were used to investigate the effect of creep and temperature on the microstructure of the material. SEM was used to examine and subsequently compare the change in microstructure as the temperature is changed. The three specimens were subjected to a stress level of 160 MPa. Figures 3.5, 3.6 and 3.7 show the SEM photographs taken for 600, 825 and 1200 °C respectively. In each case, the changes in both the axial and transverse fiber bundles were observed. At 600 °C, the fracture surface of the fibers is highly corrugated which implies brittle failure as observed in the creep curves. Most of the fibers are in the plane of the fracture and most of the fibers in the cross plies are intact. At 825 °C, the surfaces of the broken fibers are smoother implying a tendency towards ductile behavior. Another important observation is the partial or complete peeling off of the interface layer around the fibers, thus exposing them to oxidation. The interface layer does not melt completely. At 1200 °C, the fiber surfaces are completely smooth and the fiber pull out is very extensive. The fibers in the cross plies are not only broken but they exhibit multiple cracks on their cylindrical surface. Also, the fibers break at multiple positions along their length leading to small segments of broken fibers everywhere. These observations can be used to conclude that increase in temperature induces some sort of ductility in the material, which is manifested macroscopically in the failure strain. The failure strain at 1200 °C is almost double the strain at 600 °C, which implies that the material has the tendency to accumulate more strain at high temperatures. The macroscopic observations at an intermediate temperature could not be used to explain the different macroscopic creep behavior at 825 °C.

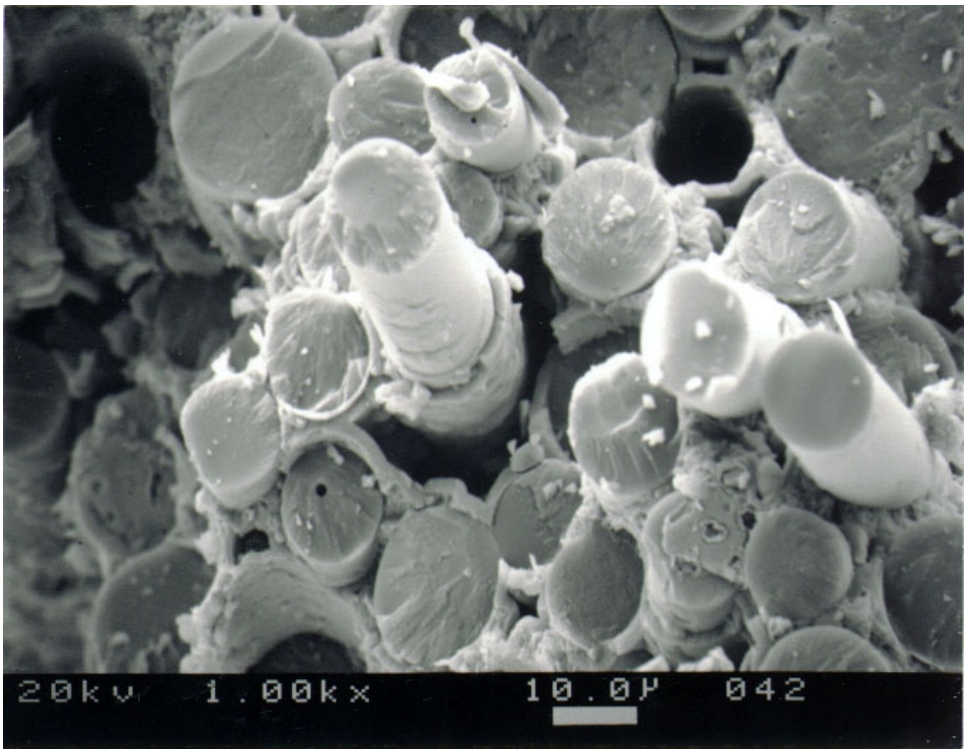

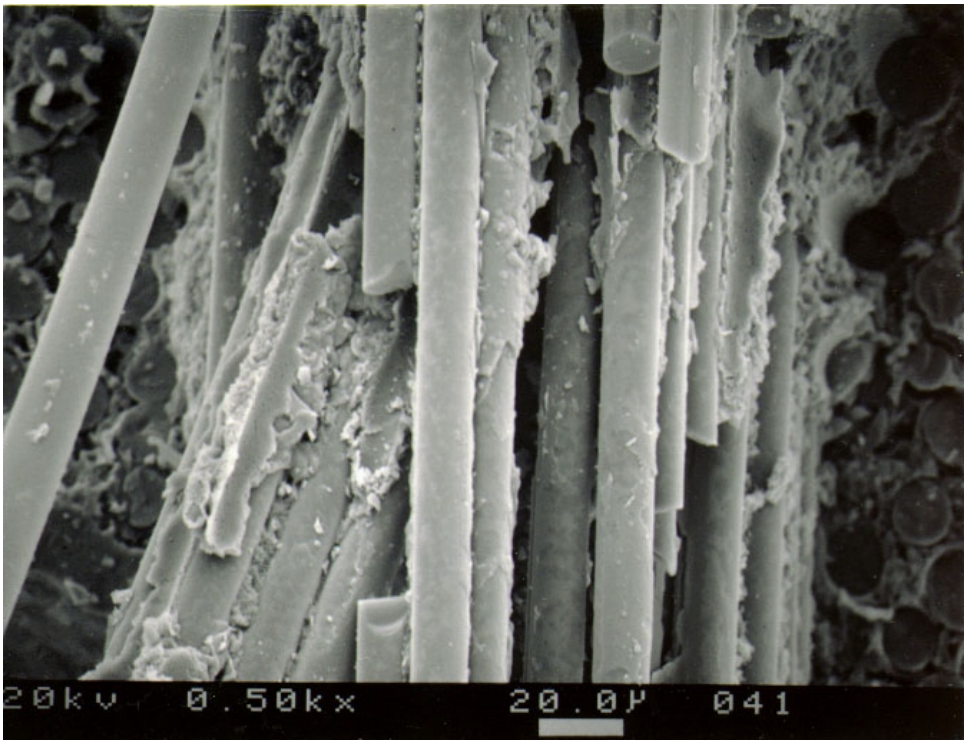

Figure 3.8— SEM photographs of the specimen fracture surface at 600 ^{0}C

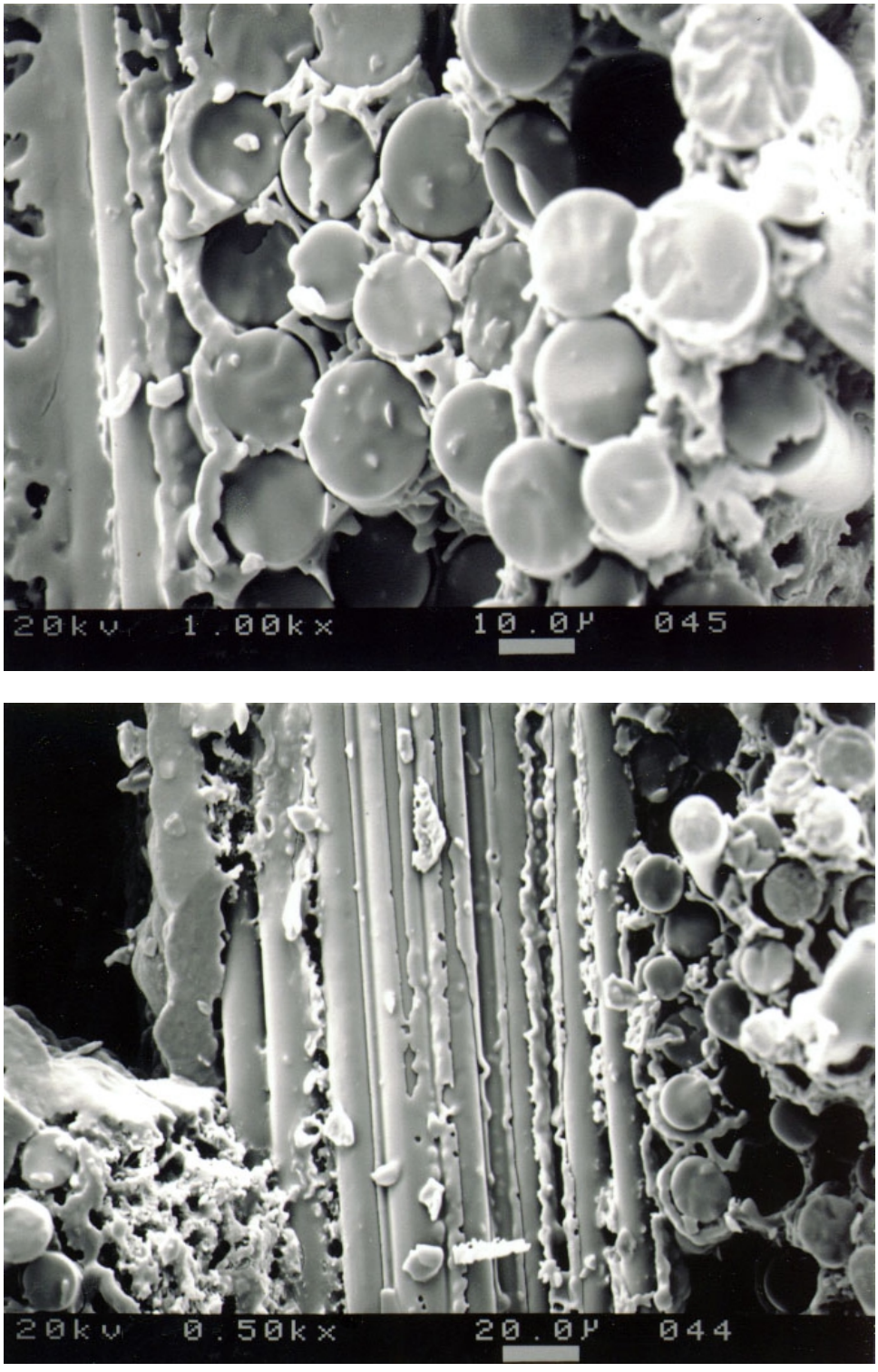

Figure 3.9— SEM photographs of the specimen fracture surface at 825 ^{0}C

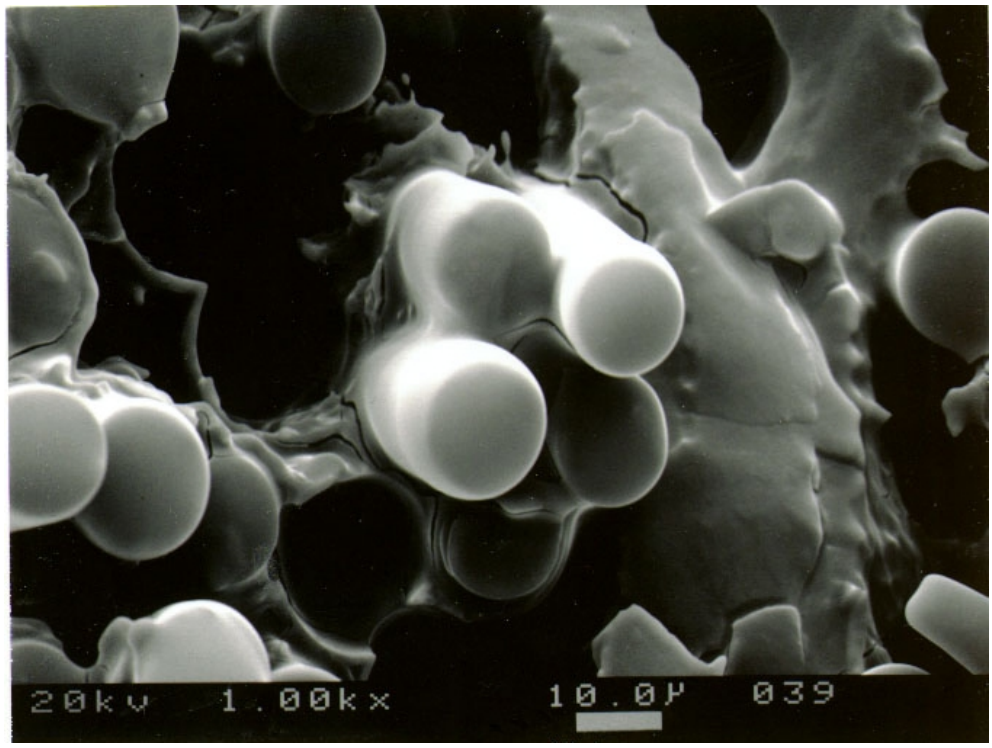

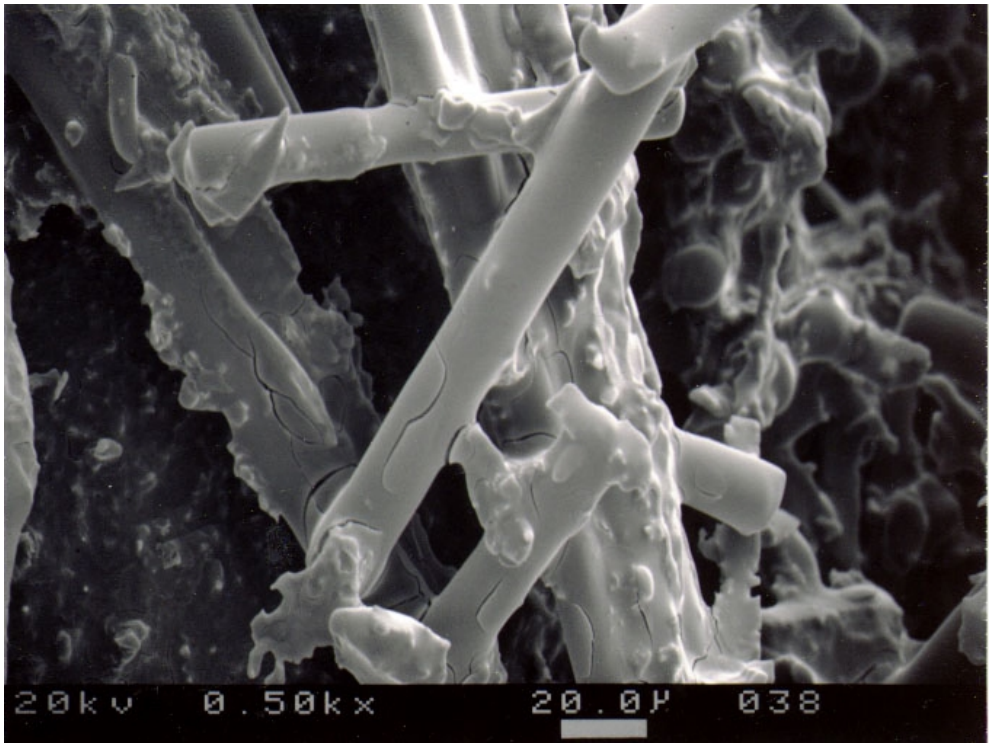

Figure 3.10— SEM photographs of the specimen fracture surface at 1200 ^{0}C

3.7. CREEP RECOVERY BEHAVIOR OF ENHANCED SIC/SIC CMC's

An experiment was conducted to investigate the creep recovery and cyclic creep behavior of the material. The specimen was loaded at 1200 °C to a stress level(140 MPa) quasi statically and held at that stress for a duration of approximately 2 hours. It was then unloaded and held at zero stress level for an equivalent amount of time. The loading and unloading rates were constant and 10-15 MPa/ sec. At the end of the recovery time, the specimen was reloaded to a higher stress level in order to find the dependence of recovery behavior on the stress level. The procedure was repeated until the specimen failed. Figure 3.11 shows the creep and recovery curves at different stress levels at 1200 °C. From the plot, it can be seen that the material has a tendency to recover the instantaneous as well as the accumulated creep strain over a period of time and the recovery behavior seems to be independent of applied load during creep.

3.5 QUASI-STATIC CYCLIC BEHAVIOR OF THE ENHANCED SIC/SIC CMCs

The strain recovery test mentioned in the previous section illuminated interesting behavior of the material during unloading. To further investigate the material behavior during unloading, a quasi-static loading-unloading test was conducted using the same experimental setup as for the creep tests. At a temperature of 1200 °C, the specimen was loaded to a stress level of 30 MPa at the same rate as used for previous tests and immediately unloaded and allowed to recover the accumulated strain. It was again loaded to a higher stress and the above procedure repeated until the specimen failed. The load was increased in steps of 10 MPa. The specimen failed at 251 MPa after 24^{th} cycle. Figure 3.12 shows the stress strain response of the material obtained from the

test. This test further confirmed the fact that the material completely recovers the inelastic strain accumulated during loading. Also, there is a very small percentage of residual strain in the material upon unloading (~2% of failure strain) which also recovers with time. This can be due to the fact that the non-linearity in the stress-strain curve and hence, the accumulation of the inelastic strain upon loading is due to fibers slipping from the matrix and therefore, when the load is removed the fibers tend to return back to the normal configuration. This behavior implies that the fibers are viscoelastic at high temperatures. Figure 3.12 shows the stress strain curves for the individual cycles. Below a stress level of 50 MPa, which has been identified as the proportional limit in the quasi-static tests, the curves do not show any hysteresis loops. As the load increases the hysterisis loops begin to show up and the area of these loops increases with loads and/or cycle. The material behavior shifts towards a bilinear stress-strain curve after a few cycles rather than being non-linear throughout the loading range. The stress at which the material changes modulus remains constant and equal to 50 MPa which shows that there is no hardening in the material. Another interesting feature upon unloading is that the stiffness of the unloading curve increases once the stress is below 50 MPa. This can be attributed to the fact that any amount of debris accumulated due to matrix/fiber breakage during loading gets into the cracks in the matrix. During unloading when the material tries to return to its original configuration by closing the cracks formed during loading, the debris offers resistance to deformation thereby increasing the stiffness. A similar test was conducted at room temperature in order to investigate the effect of temperature on the stress-strain behavior of the material. The stress-strain curve from the test is shown in figure 3.14. The behavior of the material though non-

linear at room temperature is different from the behavior at 1200 °C. The cyclic tests show that the material exhibits hardening at room temperature. Also, at room temperature, the material does not recover the permanent strain once the load has been removed completely. At room temperature, both the initial modulus and the tangent modulus change with the number of cycles whereas at high temperature, only the tangent modulus changes with the number of cycles. Figure 13.5 shows the comparison between the stress-strain curves at room temperature and 1200 °C. The initial modulus at room temperature was found to be 153 MPa, which is significantly greater than the modulus at high temperatures. The permanent strain upon unloading completely was found to be the same both the temperatures.

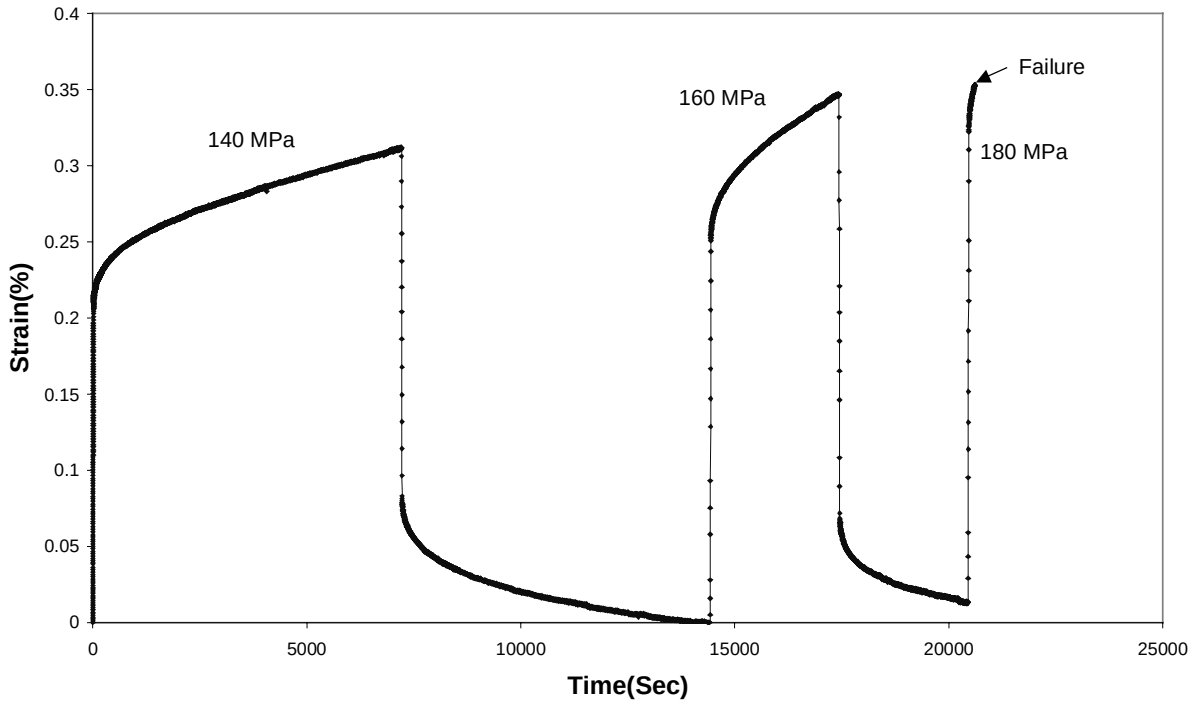

Figure 3.11— Creep Recovery behavior of the Enhanced SiC/SiC CMC at 1200 °C

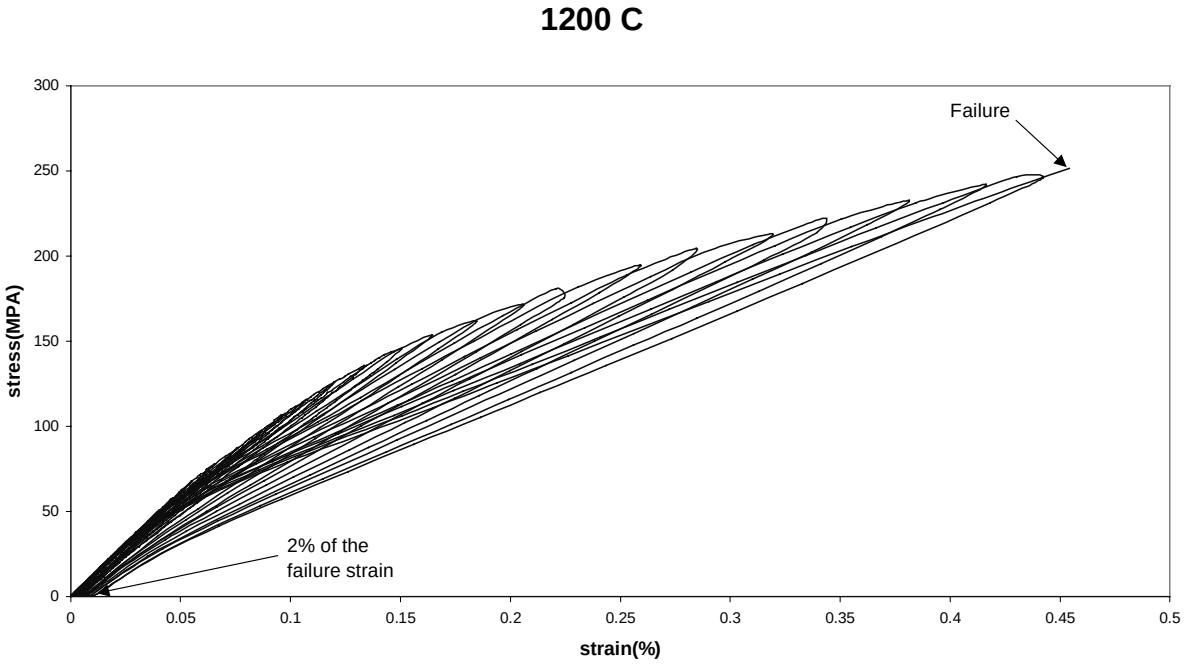

Figure 3.12— Quasi-static cyclic behavior of the Enhanced SiC/SiC CMC at 1200 °C

1200 C

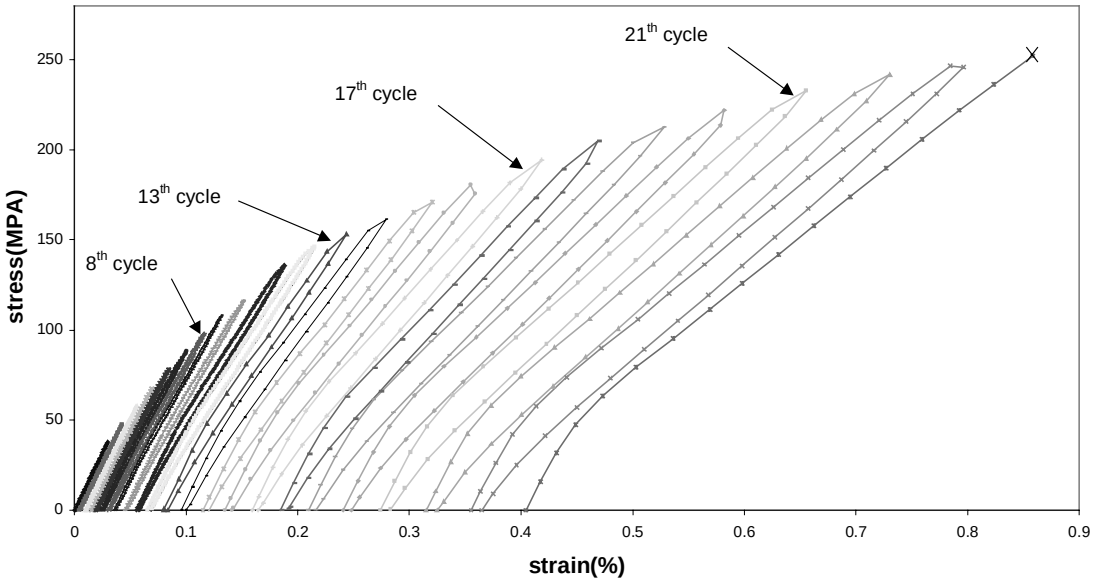

Figure 3.13— Stress-strain curves for individual cycles for the Enhanced SiC/SiC CMC at 1200 ^{0}C.

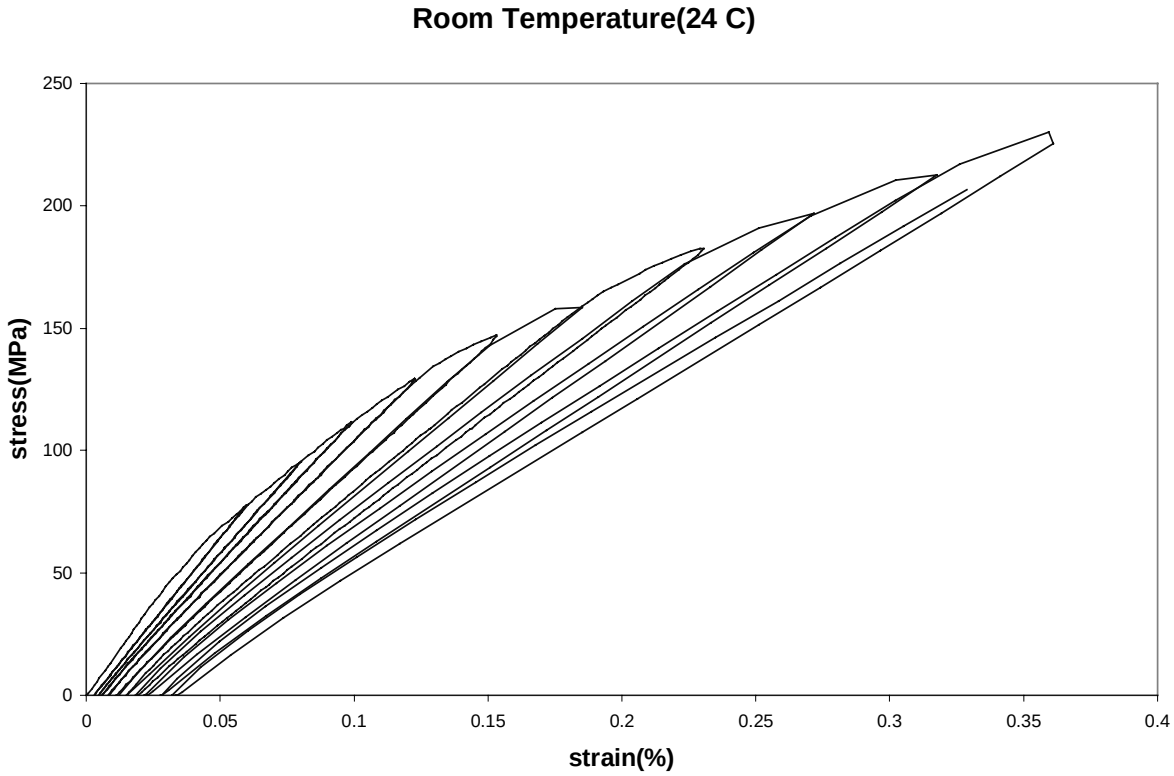

Figure 3.14— Quasi-static cyclic behavior of the Enhanced SiC/SiC CMC at Room Temperature (24 °C)

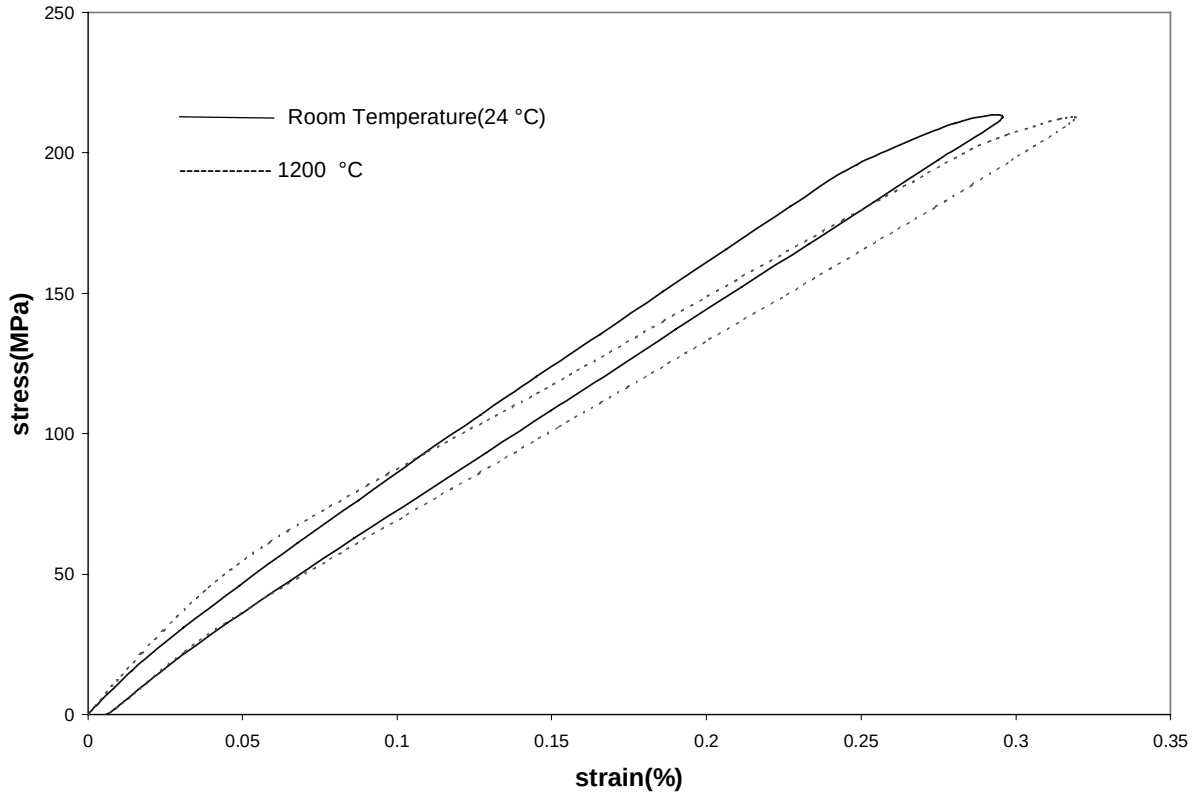

Figure 3.14— Comparison of stress-strain behavior at room temperature (24 °C) and 1200 °C

CHAPTER FOUR

4.1. REPRESENTATION OF CREEP DATA

This section describes various empirical relationships used to characterize the creep data such as rupture time and minimum creep strain rate. Figure 4.1 shows the creep rupture time versus stress data at various temperatures. These data are generally fitted to an empirical relationship of the following form

$$t_r = B.\sigma^{-N}$$

where t_r is the time to rupture(hours), σ is the applied stress(MPa), B is a constant and N is the stress exponent for stress rupture. The value of N was found to be 10.5 at 1200 °C and 13.6 at 600 °C. These values are somewhat higher than those generally reported for other CMCs. Zhu et. al. found the value of N at 1200 °C for plain weave SiC/SiC composites to be 8.1[36]. The value of N for 825 °C was not calculated due to insufficient data.

The steady state strain rate versus time to rupture data is shown in Figure 4.2. The data can be fitted to the Monkman-Grant relationship, which is given as

$$t_r \cdot \dot{\varepsilon}^m = C_{M-G}$$

where m is the strain rate exponent , t_r is rupture time(hours), $\dot{\varepsilon}^m$ is strain rate(/sec) and C_{M-G} is a material constant. This equation is commonly used to determine the creep rupture behavior in ceramics.

The value of m was found to be 0.632 which is close to the value of 0.72 as mentioned by Zhu et al. [36] but the fit to the data was not very good. The R^2 value, which is a

measure of the closeness of the data to the equation, was 0.728. Recent investigations by some researchers (Ferber and Jenkins [37], Luecke et al. [38], Menon et al. [39]) have shown that for some ceramic materials show a stratification of the MG curve

$$\ln t_f = d_1 - d_2 \ln(\dot{\varepsilon}) + \frac{d_3}{T}$$

depending on the temperature level. Menon et. al. introduced the effect of temperature by using the following equation

where d_1, d_2 and d_3 are constants. The so called Modified Monkman-Grant(MMG) equation is shown to be better at representing the data [40]. The MMG approach assumes that the strain rate exponent remains the same, but as temperature increases the curves shift up. The creep strain rate data for Enhanced SiC/SiC composite shows a different behavior because the measured strain rates at 825 °C were lower than those at 600 and 1200 °C. Hence, the curves for this material do not shift up monotonically as the temperature increases. To account for this fact, a parabolic equation was used for temperature rather than a linear equation.

The final equation can be written as

$$t_r = \left(A + BT + CT^2\right) \cdot \dot{\varepsilon}^m$$

where A,B,C and m are constants obtained from the curve fit.

Table 4.1 gives the values of the constants used in the above equation.

Table 4.1 – Values of constants used in the modified Monkman-Grant Equation

Constant	Value
A	2.95×10^{-7}
B	-4.42×10^{-2}
C	0.1663
M	1.15143

The Larsen-Miller parameter, P, can also be used to predict the creep life of these materials. This relationship between the stress-temperature-life is given as

$$P = T(C + \log t_r)$$

T is the temperature in °C

t_r is the rupture time in seconds

The constant, C, for metals and alloys is generally 20. Figure 4.3 shows the plot of the parameter as a function of stress for Enhanced SiC/SiC composite. Zhu et al. have identified the constant for SiC/SiC composites to be between 5 and 10 [36]. Using the value 7, the data can be fitted for P as a linear function of stress.

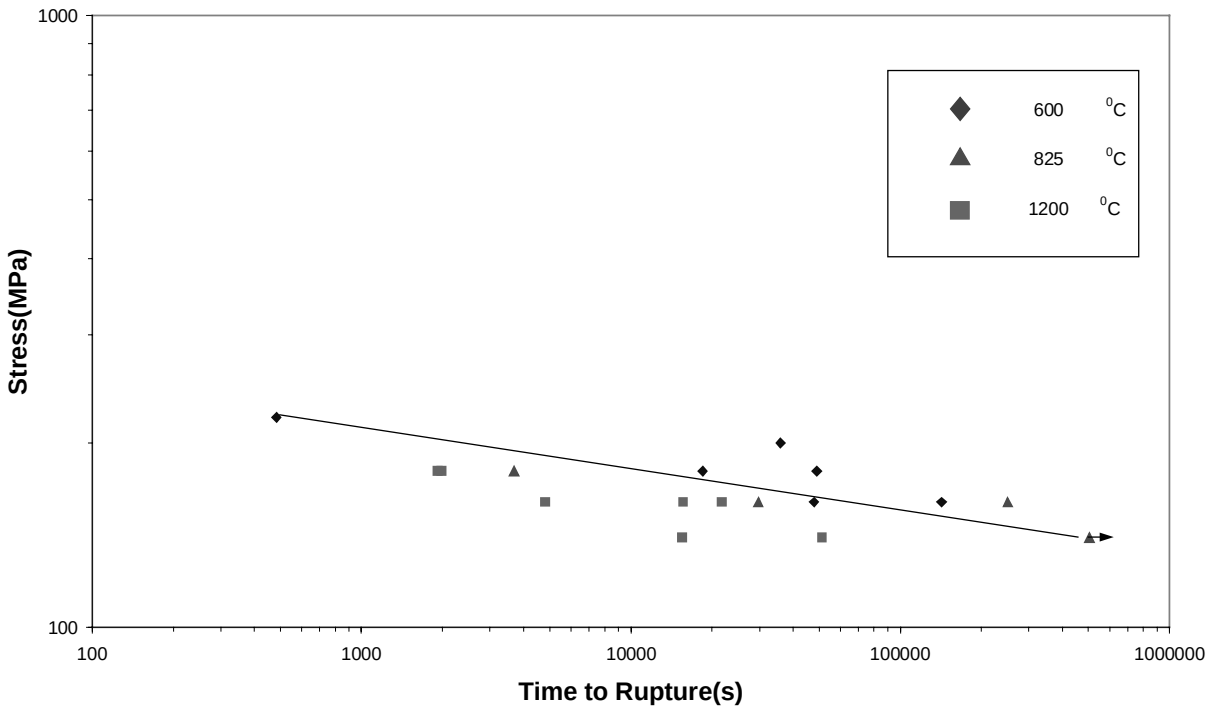

Figure 4.1— Stress Rupture behavior of the Enhanced SiC/SiC CMCs

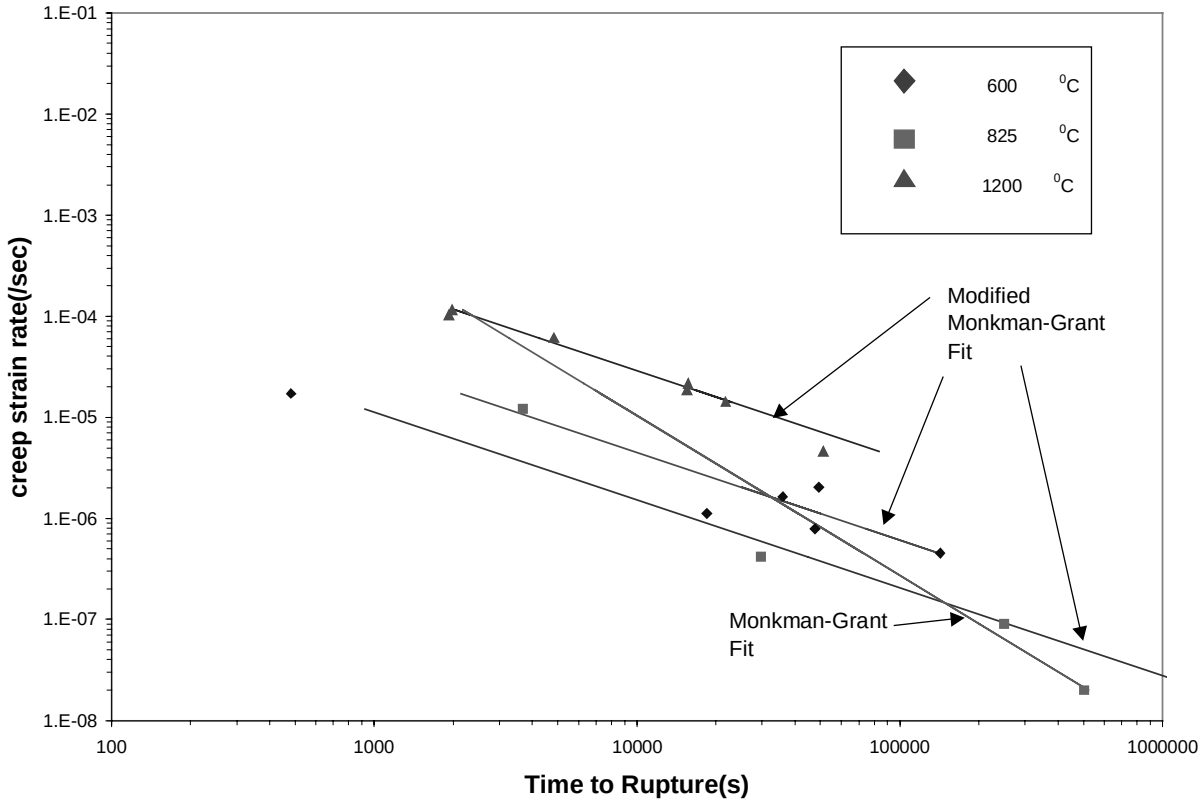

Figure 4.2— Comparison of the Monkman-Grant and the Modified Monkman Grant Relationships for the Enhanced SiC/SiC CMCs

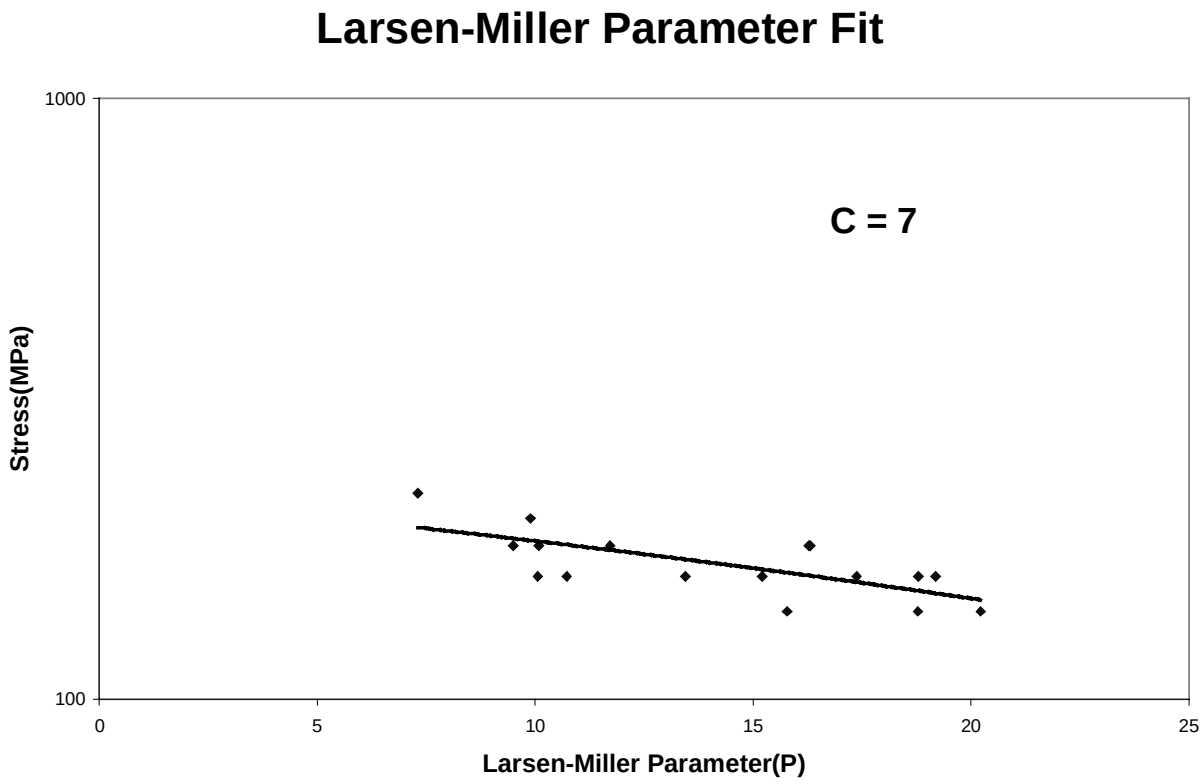

$$P = T \cdot 10^{-3}(C + \log t_r)$$

T is the temperature in °C

t_r is the rupture time in seconds

and stress is the applied stress in MPa

Figure 4.3— Tensile stress versus Larson-Miller parameter for the Enhanced SiC/SiC CMCs

4.2. REPRESENTATION OF CREEP CURVES

In the creep analysis, one of the constitutive equations is the relationship between creep strain rate and time, temperature and stress. This equation is generally written in the following form[31]:

$$\dot{\varepsilon}^c = \frac{d\varepsilon^c}{dt} = f(\sigma, T, t, \varepsilon^c)$$

The most commonly used form for the above equation is

$$\dot{\varepsilon}^c = \frac{d\varepsilon^c}{dt} = A\sigma^m t^n e^{-\left(\frac{Q}{RT}\right)}$$

In the above equation, σ is the stress, t is time, T is temperature, $\dot{\varepsilon}^c$ is the creep strain rate and A, m, n, Q, R are constants obtained from curve fitting to the data.

The above equation can be used to represent a single creep curve but if the equation is used to represent a family of curves, it is sometimes hard to find one value of the constants (m, n etc.), which can be used to represent the creep data at various stress levels and temperatures.

Hence, the equation is generally modified to fit the creep data. The creep curves for the Enhanced SiC/SiC composite as shown in Figures 3.4, 3.5 and 3.6, cannot be represented by a simple equation as the one mentioned above. The creep curves are not monotonic with temperature (the curve for 825 °C lies below the curve for 600 °C). This implies that the creep strain rate shows a minimum at an intermediate temperature. But at higher and lower temperatures, the creep strain still follows the Arrhenius rate

equation. In order to fit the data for Enhanced SiC/SiC composite, the following modifications were made.

The dependence on stress was expressed as:

$$\dot{\varepsilon}^c(\sigma) = \sigma^n$$

σ is the stress in MPa.

The dependence on time was expressed as a sum of the logarithmic terms as:

$$\dot{\varepsilon}^c(t) = \sum_{i=1}^{4} a_i \log(t)^i$$

t is the time in seconds.

Since the dependence on temperature is not monotonic, the rate term was combined with a quadratic term as shown below.

$$\dot{\varepsilon}^c(T) = (a + bT + cT^2) \cdot e^{-\left(\frac{d}{T}\right)^n}$$

T is the temperature in °C.

If we use just the quadratic term, it will not give the right results at lower temperatures. If we use just the exponential term, it gives a monotonically increasing curve. By using a combination of both and adjusting the constants suitably, we can fit the data very well. Figure 4.4 illustrates the idea.

Figures 4.5 and 4.6 show the curve fits to the creep data for the material. The total strain is plotted as a function of time and dashed lines show the curve fits.

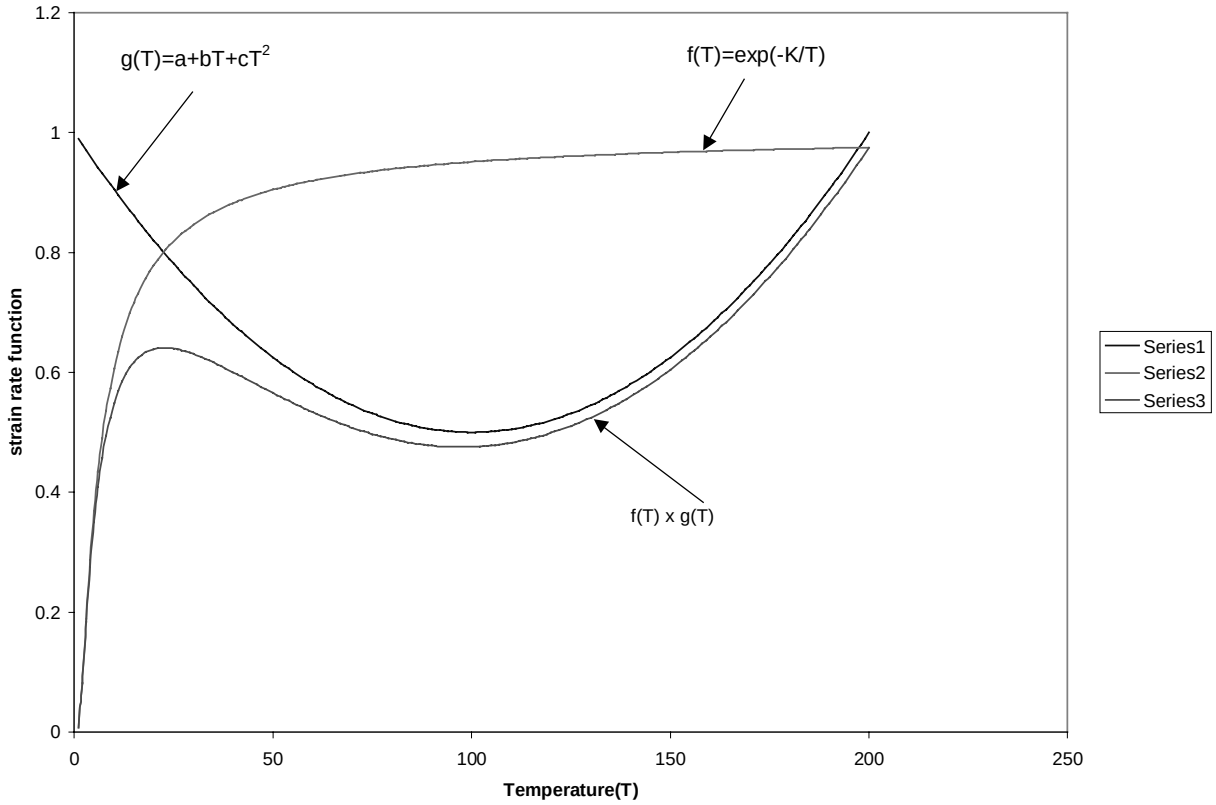

Figure 4.4— The temperature function used to fit the creep curves for Enhanced SiC/SiC composites

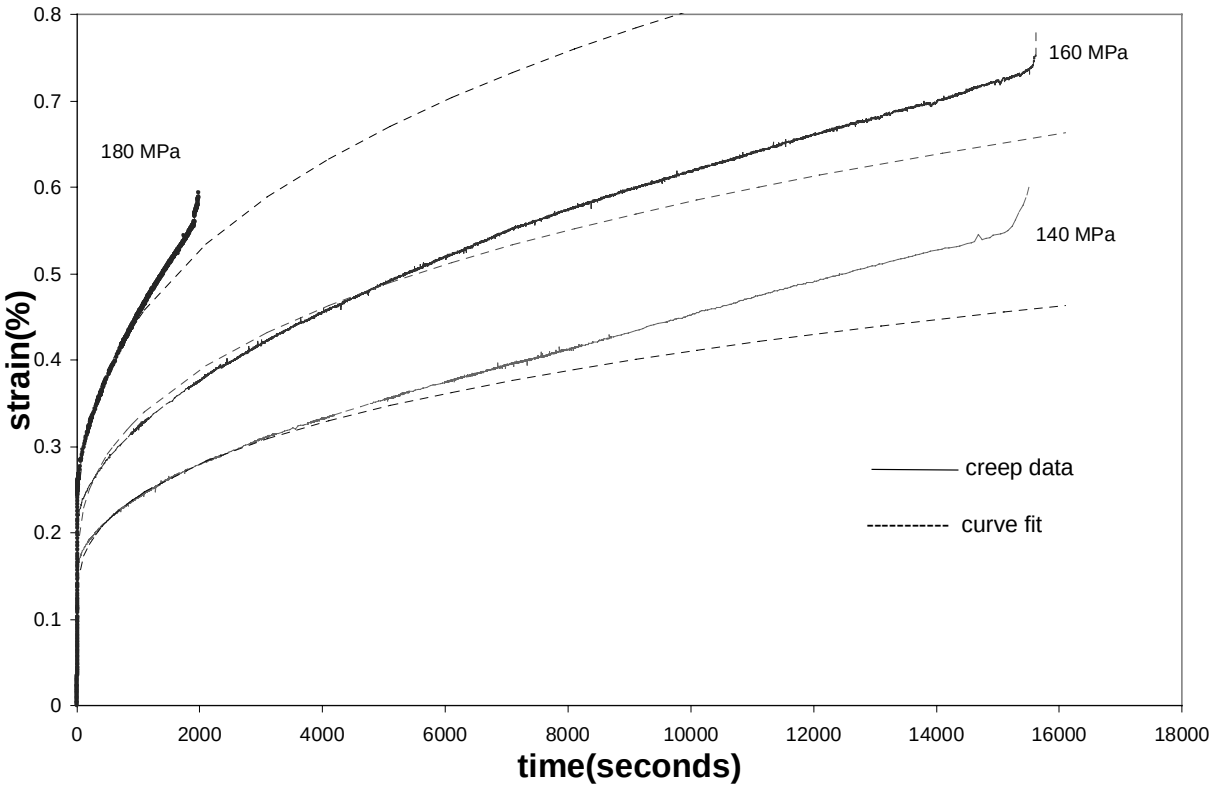

Figure 4.5— Curve fits to the creep data at 1200 ^{0}C for various stress levels

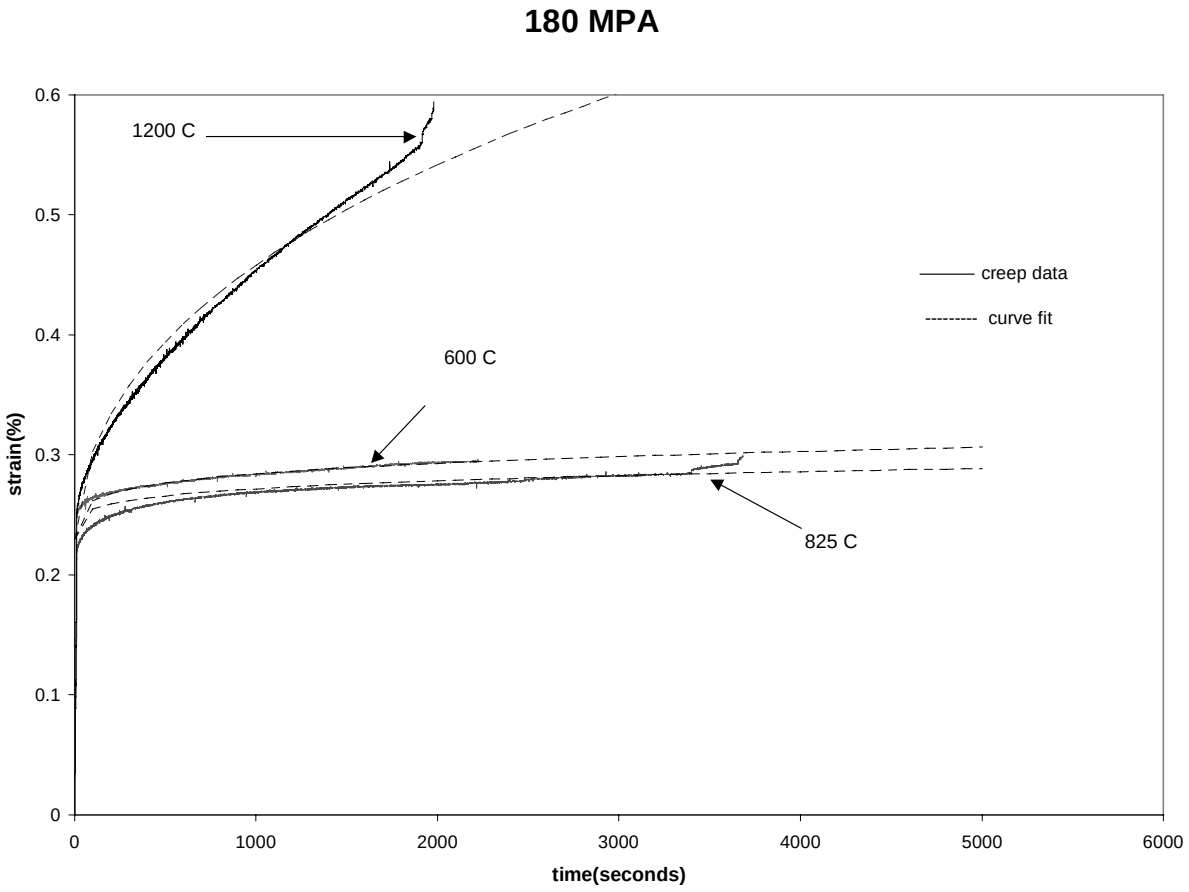

Figure 4.6— Curve fits to the creep data at 180 MPa for various temperatures

4.3. FINITE ELEMENT ANALYSIS OF CREEP BEHAVIOR

The creep response of a material can be divided into three regions: primary, secondary and tertiary. Most finite element software packages commercially available have the capability of modeling the primary and secondary regions of creep and the tertiary region is not taken into account since it implies impending failure. The creep behavior is a non-linear time dependent phenomenon and hence, an iterative procedure such as Newton-Raphson method is used to calculate the creep strain increment at each time step. Generally, an explicit procedure is used in the time stepping algorithm because of the ease and simplicity of computation.

4.3.1. CREEP ANALYSIS IN ANSYS

The creep behavior of the material was modeled using the commercial finite element Package ANSYS. In ANSYS, the solution algorithm used for creep analysis is the initial-stiffness Newton-Raphson method and the creep equations are integrated using an explicit Euler forward algorithm. The creep solution procedure described below has been taken from the theory manual provided by ANSYS [41]. The elements of the modified total strain matrix are computed for each element as

$$\left\{\varepsilon_n'\right\} = \left\{\varepsilon_n\right\} - \left\{\varepsilon_n^{pl}\right\} - \left\{\varepsilon_n^{th}\right\} - \left\{\varepsilon_{n-1}^{cr}\right\}$$

where the subscript refers to the time point n and the superscripts refer to the contribution to the strain components from plastic, thermal or creep effects. The superscript *pl* stands for plastic, *th* for thermal, *cr* for creep and the total strain is given by the term on the right side with no superscript. The term on the left hand side is the modified total strain, which is used to compute the stress.

The modified strain components are used to calculate an equivalent modified total strain given as:

$$\varepsilon_{et} = \frac{1}{\sqrt{2}}\left[\left(\varepsilon_x' - \varepsilon_y'\right)^2 + \left(\varepsilon_y' - \varepsilon_z'\right)^2 + \left(\varepsilon_z' - \varepsilon_x'\right)^2 + \frac{3}{2}\left(\gamma_{xy}'\right)^2 + \frac{3}{2}\left(\gamma_{yz}'\right)^2 + \frac{3}{2}\left(\gamma_{zx}'\right)^2\right]^{\frac{1}{2}}$$

An equivalent stress is then defined by

$$\sigma_e = 2G\varepsilon_{et}$$

where G = shear modulus = E / (2 (1+ν))

The equivalent creep strain increment ($\Delta\varepsilon^{cr}$) is calculated from the empirical relationships provided by the ANSYS or input by the user via a user defined subroutine. Some of the relations used in the ANSYS code are

$$\Delta\varepsilon_{cr} = C_1\sigma^{C_2}\varepsilon^{C_3}e^{-C_4/T}\Delta t \qquad (1)$$

$$\Delta\varepsilon_{cr} = C_1\sigma^{C_2}t^{C_3}e^{-C_4/T}\Delta t \qquad (2)$$

$$\Delta\varepsilon_{cr} = C_1\sigma^{C_2}re^{-rt}\Delta t \qquad (3)$$

$$r = C_5\sigma^{C_3}e^{-C_4/T}$$

where

ε = equivalent strain(based on modified total strain)

σ = equivalent stress

T = Temperature(absolute)

t = time at the end of substep

e = natural logarithm base

The constant C_1, C_2, C_3 etc. can be obtained by curve fitting the experimental data for any given material to the particular equation chosen for analysis.

Alternatively, if the material behavior cannot be represented by any of the relationships provided in the ANSYS, the user can define his/her own relationship and use it via a user defined subroutine and input the relationship into ANSYS.

The quantity $\Delta\varepsilon^{cr}$ is a scalar quantity and is used to define a creep ratio(C_s), which is computed for each integration point as

$$C_s = \frac{\Delta\varepsilon_{cr}}{\varepsilon_{et}}$$

The largest value of the creep ratio for iteration is output as C_{max} and is used in the automatic time stepping algorithm. Since the time increment in ANSYS is done using an explicit integration procedure, there is a stability limit placed on the time step size which is based on C_{max}. The default value is 0.10. It is recommended to use a time step size such that the value of C_{max} is less than the default value.

The creep strain increment and the equivalent strain are used to form a full strain tensor based on the number of components needed for the analysis.

The full strain tensor components are given as:

$$\Delta\varepsilon_x^{\,cr} = \frac{\Delta\varepsilon_{cr}}{\varepsilon_{et}} \frac{\left(2\varepsilon_x' - \varepsilon_y' - \varepsilon_z'\right)}{2(1+\nu)}$$

$$\Delta\varepsilon_y^{\,cr} = \frac{\Delta\varepsilon_{cr}}{\varepsilon_{et}} \frac{\left(2\varepsilon_y' - \varepsilon_z' - \varepsilon_x'\right)}{2(1+\nu)}$$

$$\Delta\varepsilon_z^{\,cr} = -\Delta\varepsilon_x^{\,cr} - \Delta\varepsilon_y^{\,cr}$$

$$\Delta\varepsilon_{xy}^{\,cr} = \frac{\Delta\varepsilon_{cr}}{\varepsilon_{et}} \frac{3}{2(1+\nu)} \gamma_{xy}'$$

$$\Delta\varepsilon_{yz}^{\,cr} = \frac{\Delta\varepsilon_{cr}}{\varepsilon_{et}} \frac{3}{2(1+\nu)} \gamma_{yz}'$$

$$\Delta\varepsilon_{xz}^{\,cr} = \frac{\Delta\varepsilon_{cr}}{\varepsilon_{et}} \frac{3}{2(1+\nu)} \gamma_{xz}'$$

The elastic strains and the total creep strains are calculated from the above tensor as follows:

$$\left(\varepsilon_{ij}^{\,el}\right)_n = \left(\varepsilon_{ij}'\right)_n - \Delta\varepsilon_{ij}^{\,cr}$$

$$\left(\varepsilon_{ij}^{\ cr}\right)_n = \left(\varepsilon_{ij}^{\ cr}\right)_{n-1} - \Delta\varepsilon_{ij}^{\ cr}$$

In the above, equation n denotes the time at substep n.

The stresses are calculated from the total strain which is calculated as $(\varepsilon_{ij}')_n$.

At the beginning of each time interval, the creep strain rate is calculated from the primary equivalent stresses and strains and is assumed to remain constant over the time interval. ANSYS uses a creep time optimization procedure, which automatically increases or decreases the time step based on the creep ratio.

Since the creep test data are obtained from rectangular specimens, the specimen geometry and dimensions were used to build the 2-D FE model to simulate the test conditions for creep behavior. Four noded quadrilateral elements were used to mesh the 2-D geometry. A model of the first quadrant of the specimen was made and symmetry boundary conditions were applied at two edges. The specimen geometry together with the boundary conditions is shown in Figure 4.5. Since the Enhanced SiC/SiC composite displays isotropic properties in the plane [6], the isotropic property option was used in ANSYS. The non-linear stress-strain curve was input in the form of a multi-linear elastic curve. This option in ANSYS allows user to represent the non linear stress strain behavior as a series of linear curves with continuously decreasing slopes. The creep constants from the curve fitting procedure were input into the material data tables for creep. Two different creep equations were used in the analysis. The first equation was the default equation for creep strain rate provided in ANSYS and the second equation was the equation obtained by curve fitting the experimental data for

SiC/SiC material. The development of this equation is described in chapter 3. The default creep strain rate equation provided in the ANSYS is given as:

$$\Delta\varepsilon_{cr} = C_1\sigma^{C_2}t^{C_3}e^{-C_4/T}\Delta t$$

The constants C_1, C_2, C_3 and C_4 can be obtained by curve fitting the above equation to the experimental data. This equation was found to be inadequate for representing the creep data for Enhanced SiC/SiC composite. The main problem was in keeping the values of C_1, C_2 etc. constant as one moved from one stress or temperature level to the another. In other words, although the above equation can be used to curve fit a single creep curve, it cannot be used to represent a family of creep curves at different stress and temperature levels.

To overcome the problem described above, one can introduce some more constants or terms in the equation and this approach was followed. As described in chapter 3, the new equation that was developed has the following form:

$$\varepsilon(\sigma,T,t) = \sigma^n\left[a\cdot\log(t)\cdot\left(c_1+c_2T+c_3T^2\right)\cdot e^{-\left(\frac{800}{T}\right)^{c4}}\right.$$

$$\left.+\,b\cdot\left(d_1+d_2T+d_3T^2\right)\cdot e^{-\left(\frac{800}{T}\right)^{d4}}\cdot\sum_{i=2}^{4}\log(t)^i\right]$$

In the above equation, stress is in MPa, time is in seconds and temperature is in °C.

The above equation can represent the experimental data obtained from the testing at all the stress and temperature levels. The complexity of the temperature term is due to the

pest behavior of the material and is explained in chapter 3. The total number of independent constants in this equation is 9. The above equation was input into ANSYS via a user-defined subroutine. This subroutine which is provided by ANSYS in the form of a fortran file named *usercr.f* allows users to input their own creep law in case the material data cannot be represented adequately by the default creep equations provided by ANSYS. Figure 4.6 shows the comparison of the creep curves obtained from the finite element analysis with the experimental data and the results from FEA show reasonable agreement with the test data. The finite element analysis tends to under-predict the creep strain even when the default creep laws are used. The analysis was run with the default creep laws and the results were same as that with the user-defined creep law. Hence, it was concluded that the under-prediction of creep strain was not due to the use of a user-defined equation. In fact, the used defined equation can be converted to the default creep laws in ANSYS by just setting some of the constants to zero. Though the creep behavior can be modeled using the above equations, the recovery behavior cannot be modeled using the above approach. The recovery data obtained from experiments shows that the material tends to behave as a viscoelastic material.

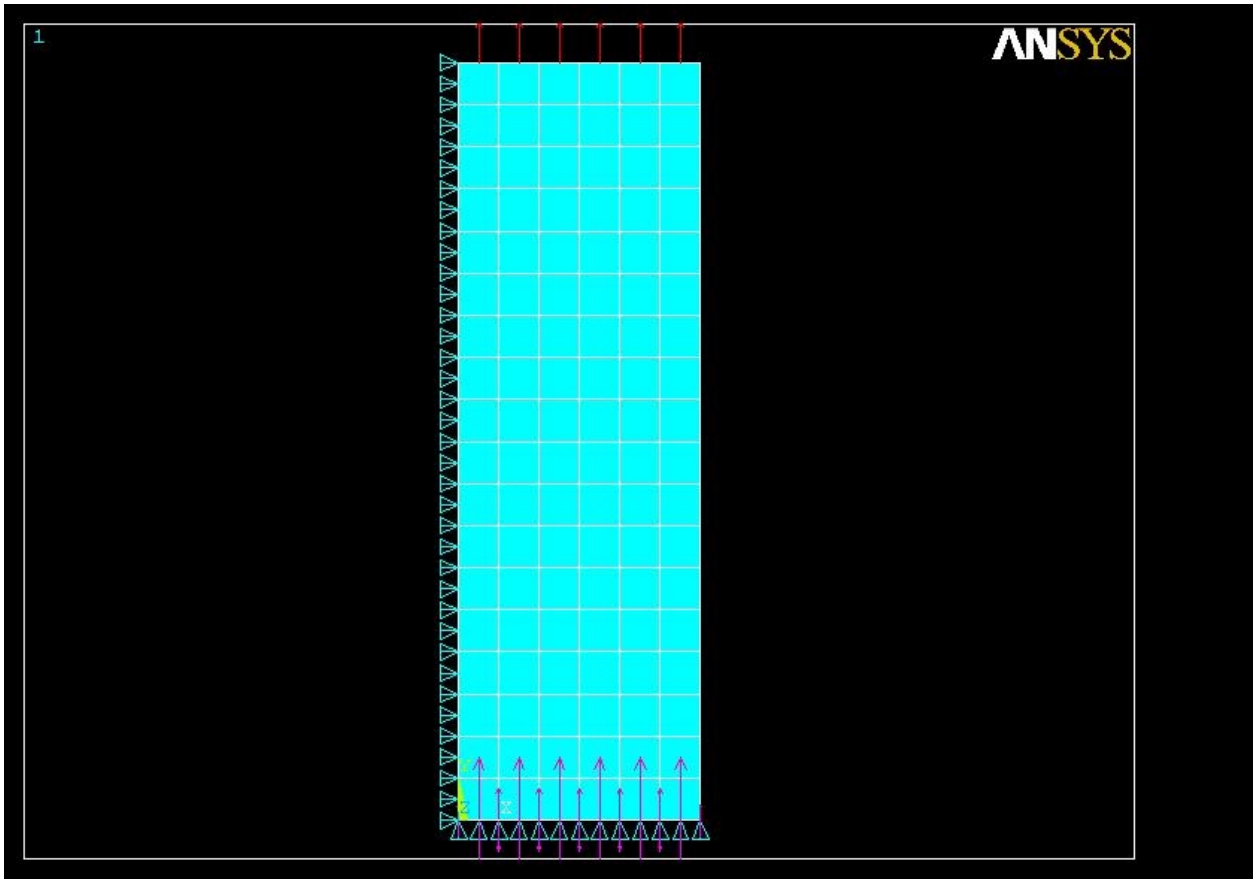

Figure 4.7— The uniform mesh and the boundary conditions used in the finite element analysis

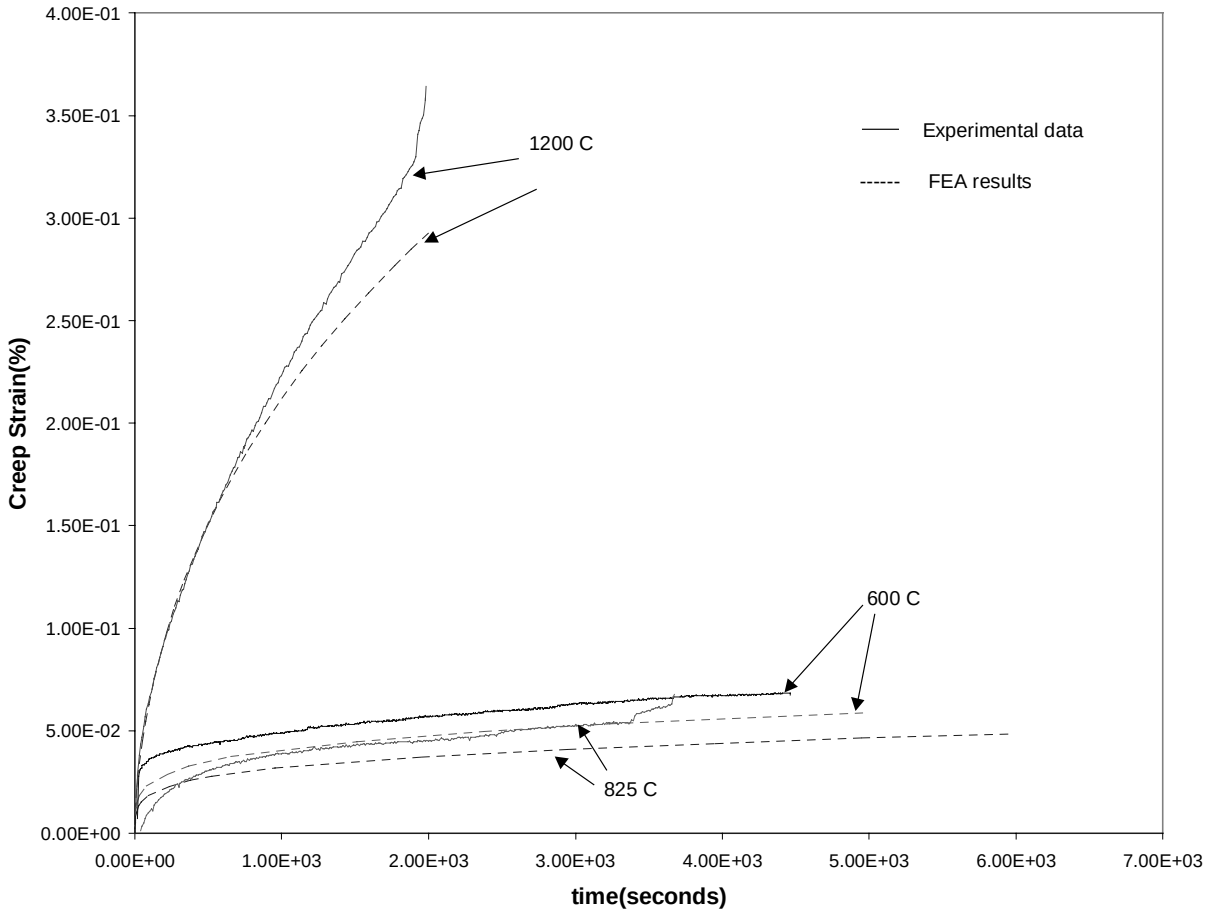

Figure 4.8— Creep strain vs time plot(comparison of the experimental data with the FEA results). The results from the finite element model under-predict the creep strain.

4.4. FINITE ELEMENT ANALYSIS OF THE QUASI-STATIC BEHAVIOR

Ceramic Matrix Composites exhibit a non-linear stress-strain behavior until failure that has been attributed to the development of cracks in the matrix and fiber-matrix interactions such as debonding and sliding. The stress-strain curve exhibits an initial linear portion upto a stress of about 50 MPa, which has been identified as the onset of matrix cracking. Beyond this stress, the modulus of the composite decreases continuously and upon unloading, a small amount of residual strain is present in the material. The cyclic behavior of the composite shows a bilinear loading curve with the development of the hysterisis loops with the number of cycles. Also, the material shows no apparent hardening i.e. the point in the stress strain curve where the modulus changes remains constant. To model the stress-strain behavior of CMC's, a representative or idealized stress-strain curve was identified which is shown in Figure 4.7. Several interesting and important observations were made from the experimental data as shown in chapter 3, Figures 3.9 and 3.10. These features are:

- Bilinear behavior during loading
- No change in the initial modulus(E) of the curve with the number of cycles
- The stress at which the modulus of the curve changes remains constant. This can be viewed as the "yield point" of a plasticity model being constant, which implies no hardening in the material.
- The tangent modulus(E_T) decreases with the number of cycles.
- Approximately linear behavior during unloading
- Small amount of permanent strain in the material upon complete unloading.

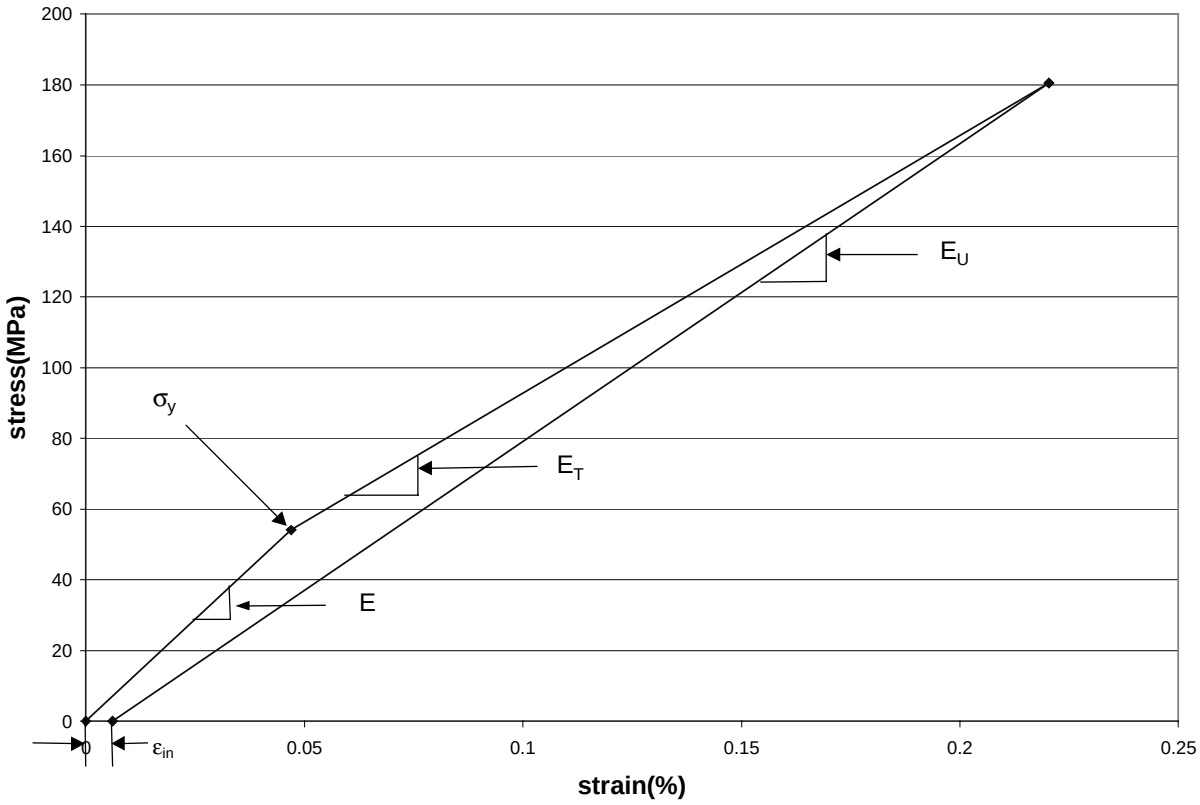

Figure 4.9— Idealized stress-strain behavior of the Enhanced SiC/SiC composite

- The unloading modulus(Eu) is dependent on the loading history.

Several of the above features such as the non-linear loading behavior of CMC's can be modeled using the concepts from the theory of plasticity such as the classical bilinear kinematic hardening rule. However, the various hardening rules present in the plasticity theory cannot predict the unloading or the hysterisis behavior of the CMC's. Hence, the rules must be modified in order to correctly predict the stress-strain curve. In order to modify the plasticity rules, it is important to understand the concepts of plasticity. The next section, which has been taken from the ANSYS theory manual, describes some of the important aspects of the theory of plasticity.

4.4.1 THEORY OF PLASTICITY

Plastic behavior of materials is characterized by the presence of irrecoverable strains on load removal as opposed to non-linear elasticity. The non-linear behavior on loading alone does not determine the plastic response [31]. The mathematical representation of the plasticity theory has three main features: the yield criterion, the flow rule, and the hardening rule [41]. The yield criterion determines the stress level at the onset of yielding. The yielding can occur only if the stresses satisfy a general yield criterion

$$F(\sigma, \kappa) = 0$$

where κ is a hardening parameter.

For a multi-axial state of stress, the above function can be interpreted as an equivalent stress(σ_e) given as

$$\sigma_e = f(\{\sigma\})$$

where $\{\sigma\}$ is the stress vector.

When the equivalent stress is equal to a material property given as yield stress(σ_y), the material will start accumulating plastic strains. If the equivalent stress is less than the yield stress, the material behavior will be elastic.

The flow rule determines the direction of the plastic straining and is given as[41]:

$$\{d\varepsilon^{pl}\} = \lambda\left\{\frac{\partial Q}{\partial \sigma}\right\}$$

where

λ is a constant called plastic multiplier and

Q is a function of stress termed as plastic potential.

The hardening rule states the conditions for subsequent yielding by describing the changing of the yield surface with progressive yielding. Two hardening rules are most commonly used: (work or isotropic) hardening and kinematic hardening. In work hardening, the yield surface remains fixed about its initial centerline and expands in size with progressive yielding. In kinematic hardening, the yield surface remains constant in size but translates in stress space as the material accumulates plastic strain.

The stress-strain curves for the two hardening rules are shown in Figure 4.7.

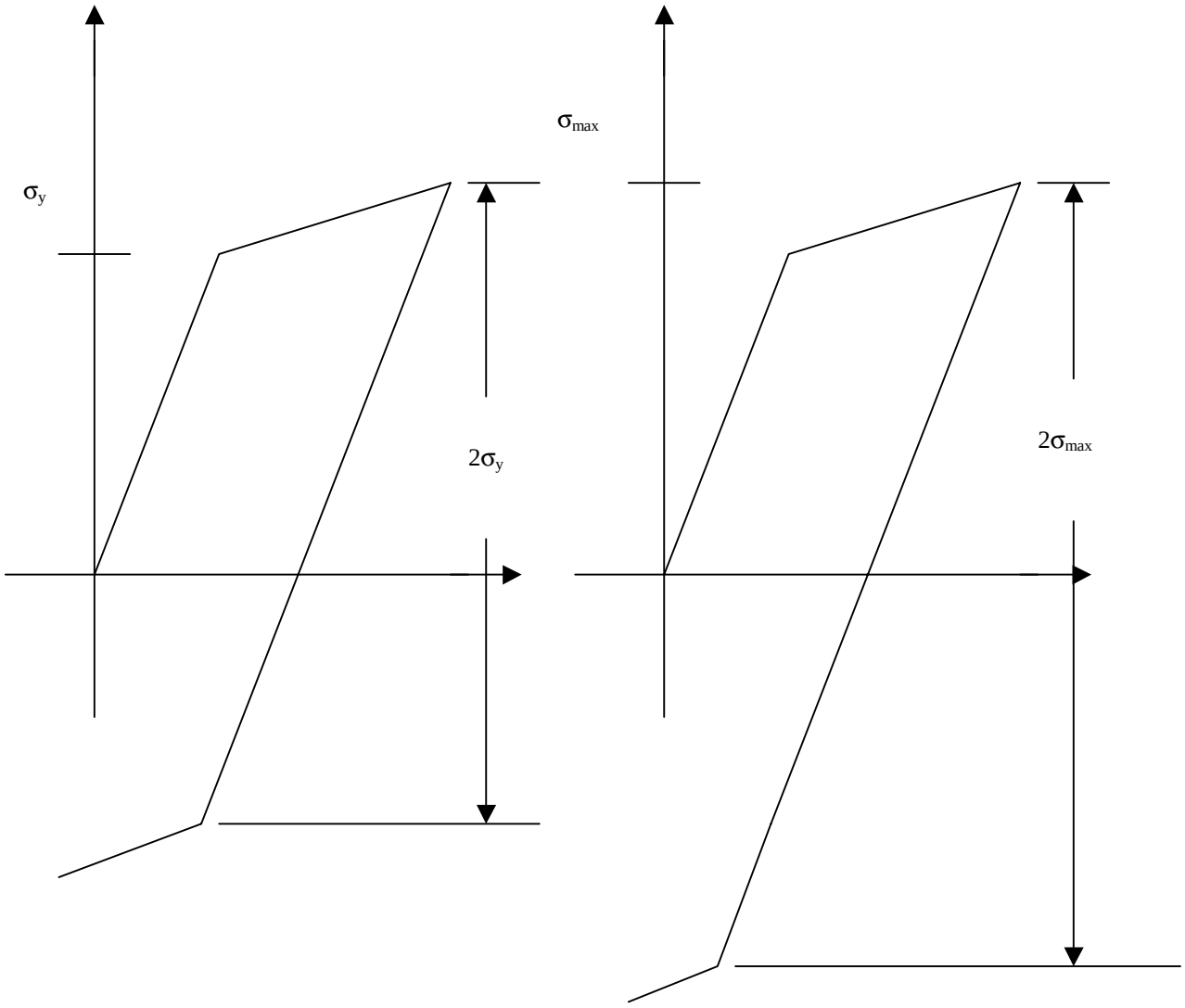

Bilinear Kinematic Hardening

Bilinear Isotropic Hardening

Figure 4.10— Stress-strain behavior for the hardening rules in plasticity

In the plasticity theory, the change in the total strain is divided into a plastic component($d\varepsilon^{pl}$) and an elastic component($d\varepsilon^{el}$).

$$\{d\varepsilon\} = \{d\varepsilon^{el}\} + \{d\varepsilon^{pl}\}$$

The increments in stress are computed via the elastic stress-strain relations as

$$\{d\sigma\} = [D]\{d\varepsilon^{el}\} = [D](\{d\varepsilon\} - \{d\varepsilon^{pl}\})$$

Where [D] is the matrix of the elastic constants and the increment in the plastic strain is calculated from the flow rule.

4.4.2. MODELING THE STRESS STRAIN BEHAVIOR OF SIC/SIC COMPOSITES

The stress strain behavior of SiC/SiC composites as observed from the experimental data was idealized as shown in Figure 4.6. Since the material exhibits isotropic behavior in a plane [6], the isotropic properties were used in the finite element analysis. The bilinear kinematic hardening rule was modified in order to model the stress-strain behavior. The commercially available finite element software ANSYS was used to perform the analysis. ANSYS has a capability of allowing the users to input their own constitutive laws via a user-defined subroutine. These subroutines are generally written by the software suppliers to model some known material behavior such as elasticity, plasticity, or viscoelasticity and hence the basic code is supplied to the user. The user can then modify the existing code to model any new material behavior. In the present study, the user subroutine "*userpl.f*" was used to model the stress-strain behavior of SiC/SiC composites. This subroutine demonstrates the numerical scheme for the

classical bilinear kinematic hardening rule. This option uses the Von Mises yield criterion with the associated flow rule and kinematic hardening. The equivalent stress is defined as

$$\sigma_e = \left[\frac{3}{2}\left(s_{11}{}^2 + s_{22}{}^2 + s_{33}{}^2 + 2s_{12}{}^2 + 2s_{23}{}^2 + 2s_{13}{}^2\right)\right]^{\frac{1}{2}}$$

Where s_{ij}, i,j=1..3 are the components of the deviatoric stress vector.

The yield criterion is therefore

$$Q = \sigma_e - \sigma_Y = 0$$

Where σ_e is defined above and σ_y is the yield stress obtained from uniaxial tensile experimental data. The flow rule then becomes

$$\left\{\frac{\partial Q}{\partial \sigma}\right\} = \frac{3}{2\sigma_e}\{s\}$$

An important feature of the user subroutine is the capability of defining and storing information using the internal or state variables. In the subroutine *userpl.f*, one can store upto six different quantities in state variables. From Figure 4.6, the unloading modulus can be defined as

$$E_u = \frac{\sigma_{\max}}{\varepsilon_{\max} - \varepsilon_{in}}$$

In the above equation, σ_{max} is the maximum stress in an element during loading, ε_{max} is the corresponding strain and ε_{in} in the inelastic strain upon completely unloading.

In plasticity computations, the total load is applied in increments and hence, a load step is divided into a number of sub steps. At the end of each load sub step, the stress and total strain are stored in the state variables. These state variables are updated after every sub step so that the maximum value of stress and strain is stored in them. When unloading occurs, the values in the state variables are the maximum stress(σ_{max})and strain(ε_{max}) at an integration point in an element. These values are used to calculate the unloading modulus and hence each integration point unloads along a modulus, which depends on the maximum stress at that point during loading. This implies that each element has a different unloading modulus, which is dependent on the maximum stress in the element during loading. At the beginning of each substep, a check for loading or unloading is made by one of the two options described below:

- In ANSYS, one can apply a forced boundary condition via load steps. In a given load step, one can either increase or decrease the applied external load but not both. Hence, the load step number can be used to determine when the external load is increasing or decreasing and based on that information, one can check for loading or unloading.
- At the beginning of each sub step, the trial stresses are calculated from the elastic strain and hence the stress in a given sub step can be compared with the stress from the previous sub step(stored in the state variables). If the stress in the current sub step is greater than the stress in the previous sub step, loading occurs and if it is lesser, unloading occurs.

The first procedure (although not very logical) gives better convergence. This is because in non-linear analysis, the solution is achieved through a series of iterations.

Often while converging to a solution, the trial solution might not approach the true solution from one direction. In other words, the stresses in the intermediate iterations might be either greater or lesser than the stresses from the previous sub step, which leads to convergence problems if the second option is used. Once the check for unloading has been made, the unloading modulus can be calculated and the new strains can be calculated using the unloading modulus.

The above procedure was incorporated into the user subroutine and input into ANSYS. The simulations were run on a model shown in figure 4.5 and the results were compared with the test data. Figure 4.8 shows the comparison of the results from the finite element analysis with the experimental data. The results are also compared with the default plasticity option (BKIN) available in ANSYS, which models the classical bilinear kinematic hardening rule. The finite element results using the userpl.f algorithm agree closely with the experimental data for both the loading and the unloading behavior. On the other hand, though the default BKIN option in ANSYS matches the test data for the loading portion of the curve, there is a significant difference in the unloading portion of the curve as compared with the test data.

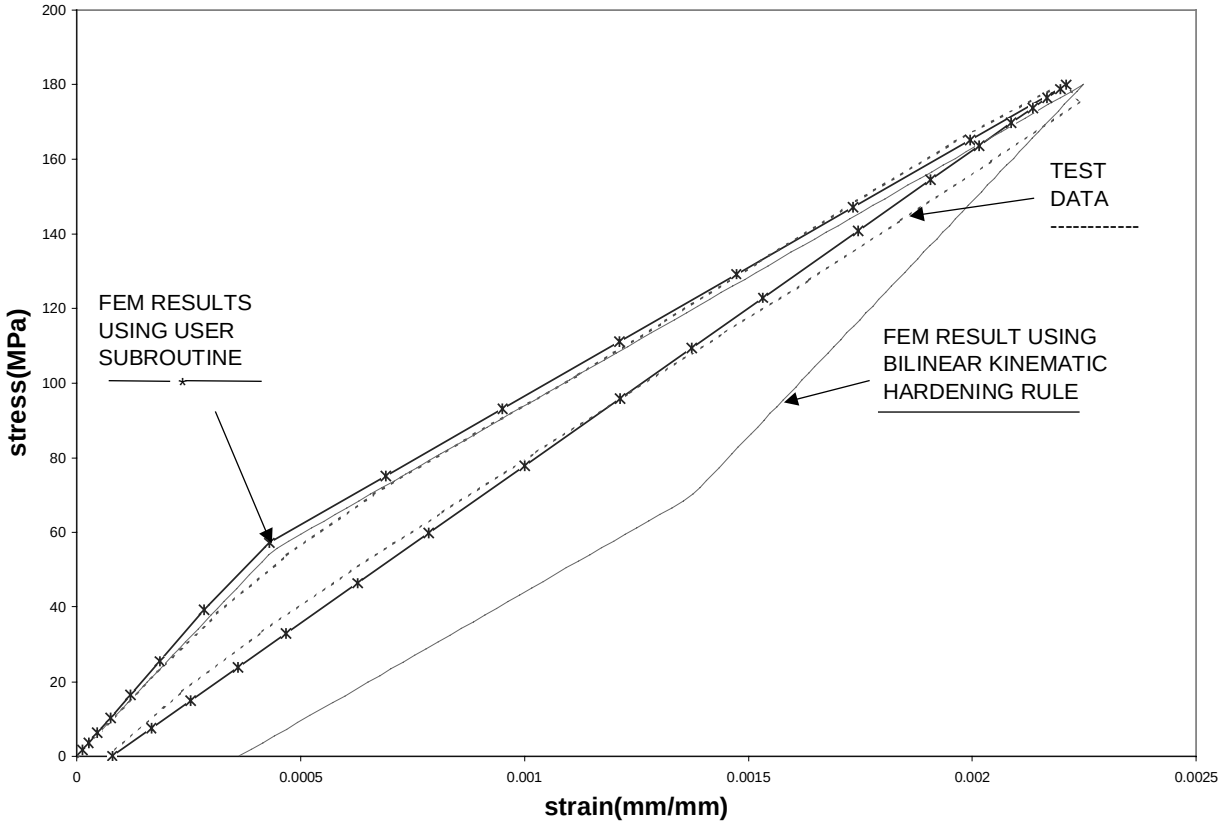

Figure 4.11 – Comparison of the stress-strain curves obtained from the finite element analysis with the experimental data

4.4.3. MODELING THE QUASI STATIC CYCLIC BEHAVIOR OF ENHANCED SIC/SIC COMPOSITES

The quasi-static cyclic behavior of the material is shown in Figure 3.10. The main features of kind of behavior are the change in the tangent modulus(E_T) of the bilinear curve with the number of cycles and the no change in the “yield stress” with the number of cycles. The curves change slope at a stress of 50 MPa and this stress value remains constant irrespective of the number of cycles. These two aspects were incorporated into the user subroutine in order to model the effect of the cyclic behavior. The tangent modulus of the material is plotted as a function of the number of cycles(N) in Figure 4.9. A curve fit to this data was obtained by using an empirical equation of the following form:

$$E_T(N) = K.\left(1 + e^{\left(-\left(\frac{N}{N_0}\right)^{\alpha}\right)}\right)$$

where K, N_o and α are the constants obtained from curve fitting procedure. This equation does not represent the change of modulus with the number of cycles due to the fact that the maximum applied load is not constant with the number of cycles. But the main objective was to study the effect of the change in modulus and find out if this technique works. This equation was then input into the user subroutine. The number of cycles in the analysis was identified with the loadstep number. Two loadsteps are equal to one cycle as the external load is ramped up in the first step and then ramped down in the second step. Also, the yield stress was input as a constant value. Figures 4.13 and

4.14 show the comparison between the finite element results and the test data and the results match closely.

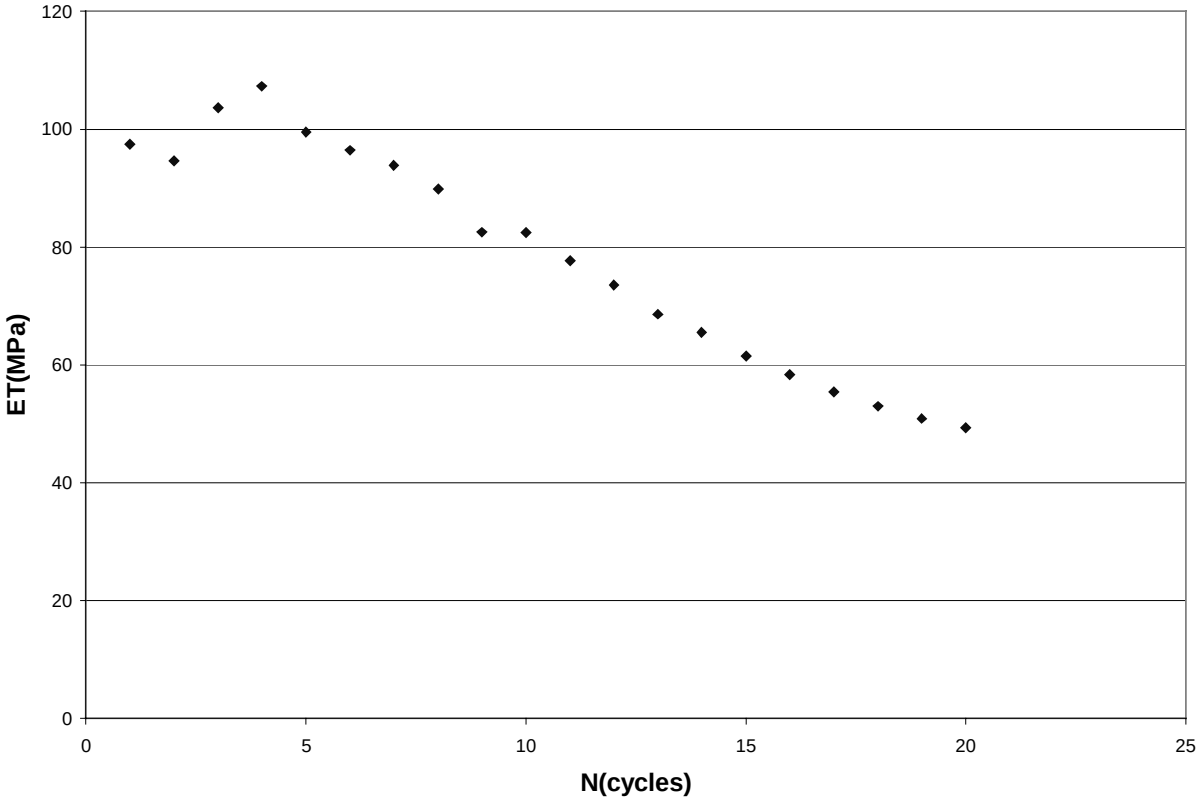

Figure 4.12 – Variation in the tangent modulus(ET) with the number of cycles for Enhanced SiC/SiC composite. This data has been obtained from quasi-static cyclic testing where the specimen was loaded and unloaded with progressively increasing load.

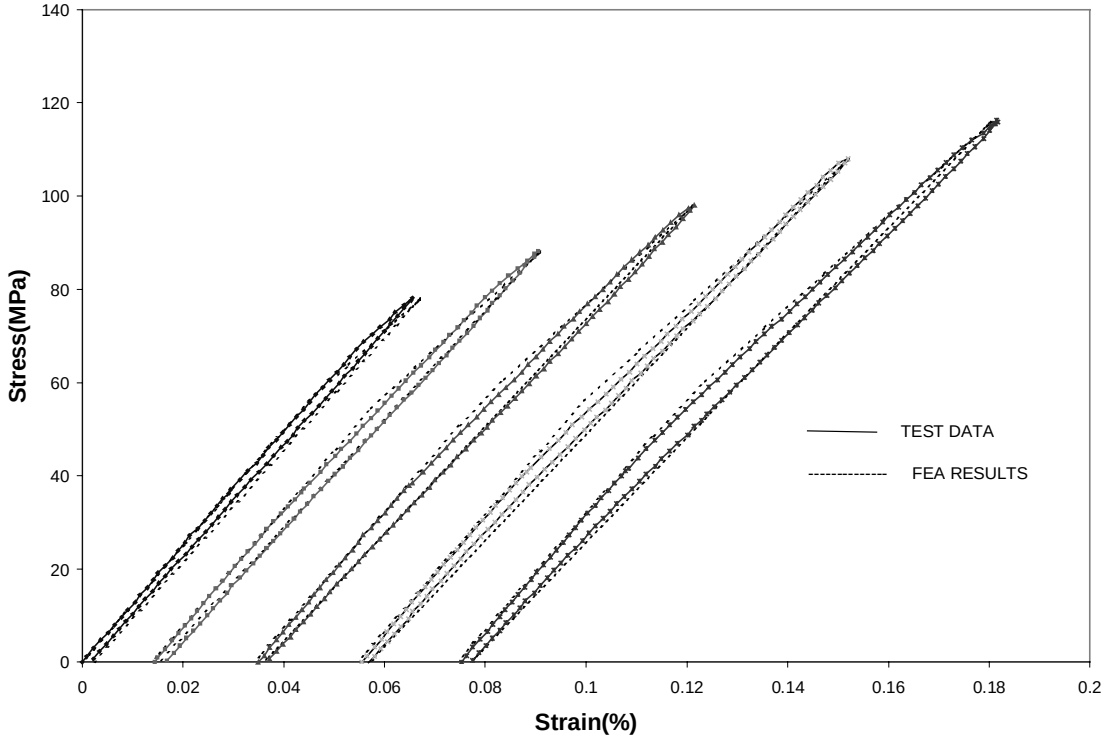

Figure 4.13 – Comparison of the finite element results with the test data for 5 cycles. The curves have been shifted along the strain axis for clarity.

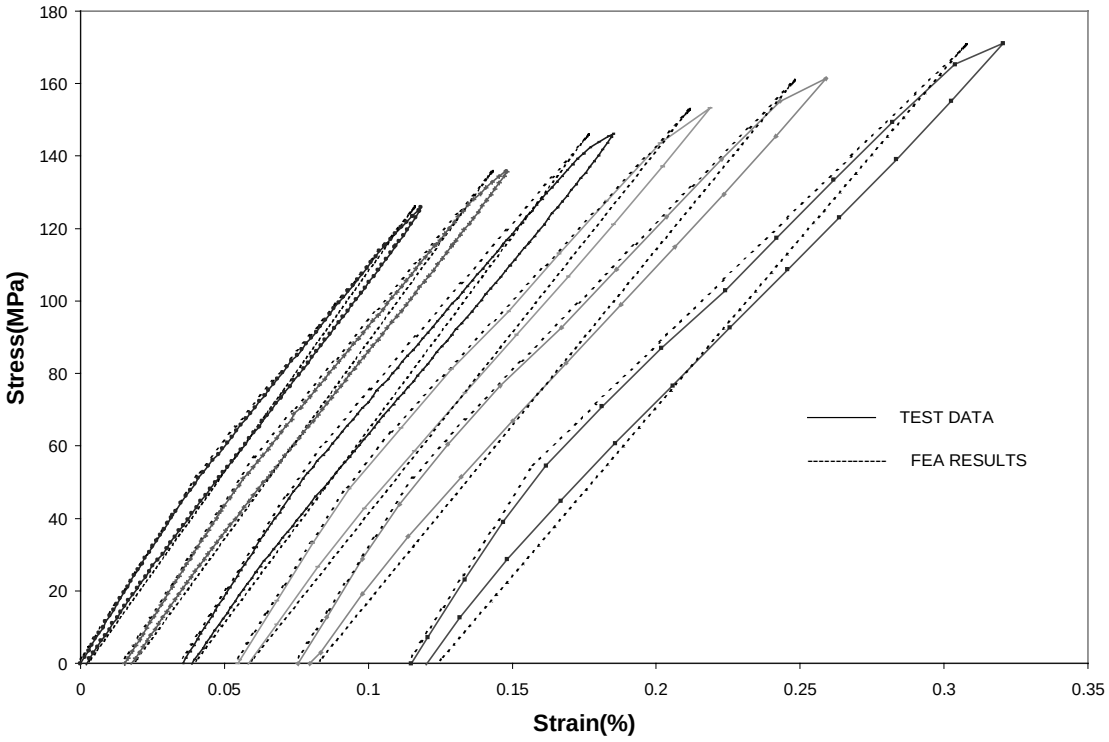

Figure 4.14 – Comparison of the finite element results with the test data for next 5 cycles. The curves have been shifted along the strain axis for clarity.

CHAPTER FIVE

5.1. INTRODUCTION

The effect of geometric discontinuities such as notches and holes is very significant in the behavior of structural components. This chapter describes the experimental work and the extension of the model used in the previous chapter to predict the stress-strain behavior of a notched specimen. The specific objective of this study was to observe the stress-strain behavior of a double notched specimen made of Enhanced SiC/SiC composite, particularly the behavior near the notch and then compare the experimental results with the prediction made by finite element analysis.

5.2. EXPERIMENTAL PROCEDURE

The test was conducted in air at room temperature (approximately 70 °F). Two semicircular notches were made on the either side of a dog bone shaped specimen using a cylindrical diamond burr. The specimen geometry is shown in Figure 5.1. The testing equipment was the same as that used for tensile and creep testing as described in chapter 3. An extensometer and two strain gages were used to measure the strain. The extensometer was placed in such a way that it encompassed the notches. The strain gages were placed near the notch and parallel to the loading direction. Since the surface of the specimen is very undulating, an epoxy adhesive was used to create a smooth surface so that the strain gages could be put on the specimen. The epoxy was cured for 2 hours at 75 °F and then the excess epoxy was removed by sand paper to make a smooth leveled surface. Once the notches were made, the available width for mounting strain gages was 0.1875 inches. Hence, only two strain gages could be accommodated in between the two notches. The strain gages were 0.08 inches wide.

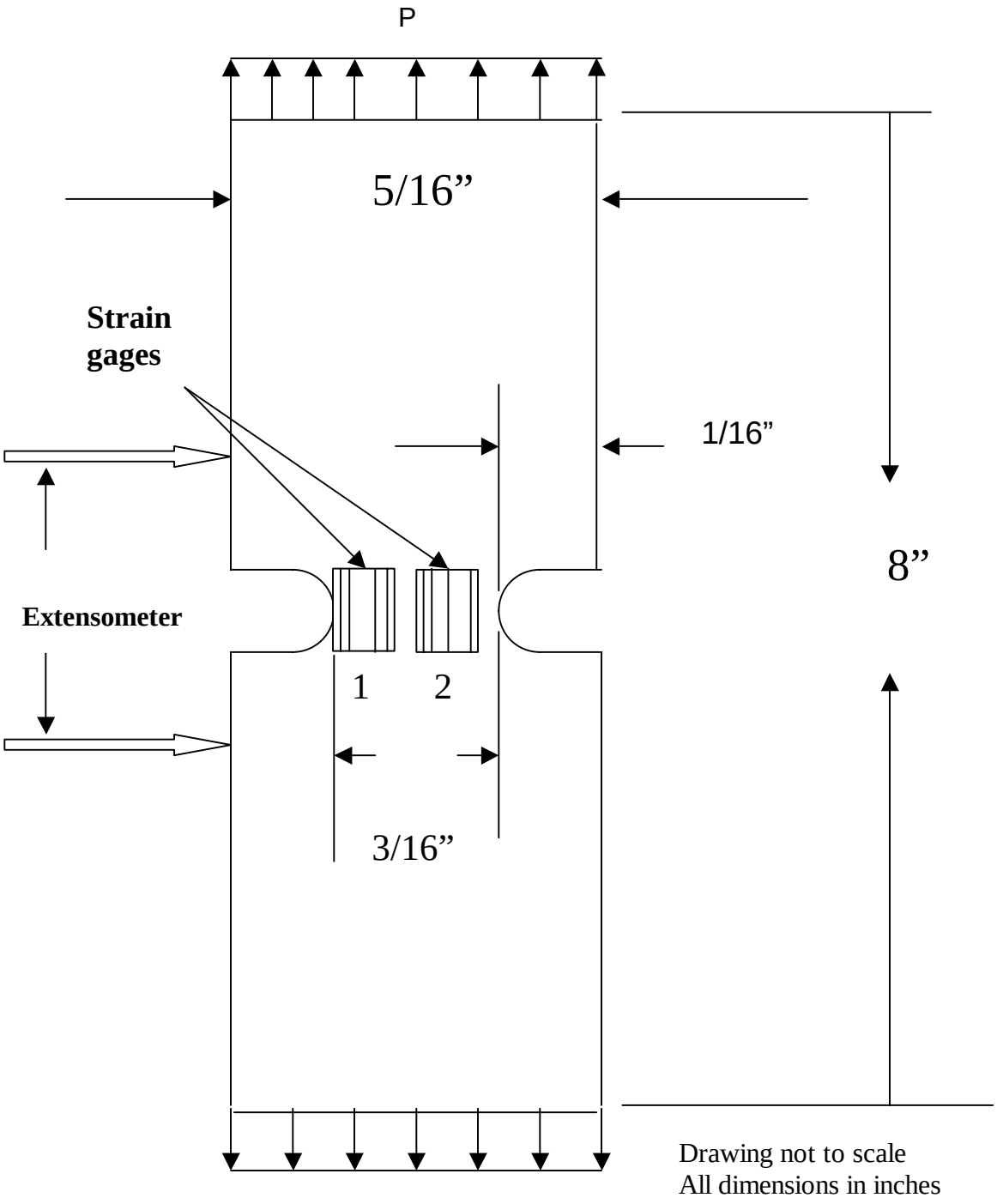

Figure 5.1—Specimen Geometry for a double notched specimen

5.3. RESULTS AND DISCUSSION

The data available from the test includes the applied load and the strain measured from the extensometer and the two strain gages. The stress is calculated by dividing the load by the original cross section area. Figure 5.2 shows the stress-strain plots at three different locations. Curve labeled 1 is the plot of remote stress vs the strain measured by the strain gage number 1(see figure 5.1). Curve 2 is the plot of remote stress vs the strain measured by the strain gage number 2(see figure 5.1). Curve 3 is the plot of remote stress vs the strain as measured by the extensometer, which encompasses the notches. These plots indicate that near the hole, the deformation is much higher than far from the notch, indicating the strain(or stress) concentration near the notch. The strain concentration is around 1.5, which is much less than the value of about 4.5 from the elasticity solution. But a closer look at the specimen geometry and the width of strain gages reveals that the readings from the strain gages might be average values rather than actual values. The net section width is 0.1875 inches whereas the grid width of the strain gage is 0.08 inches. The ratio of strain gage width to the net section width is 0.43, which is very high. Hence, there is a high probability that the strain measured by the strain gage is an average value. Also, the strain measured by the extensometer is also averaged over a length of one inch, which also includes the notches. So, there is a reason to expect much lesser strain concentration. Another interesting feature is that the stress-strain curves are almost linear over the entire range, which is different from that of un-notched specimens. The area of the hysterisis loop is much higher near the notch which indicates the presence of much higher residual strains near the notch than far from the notch.

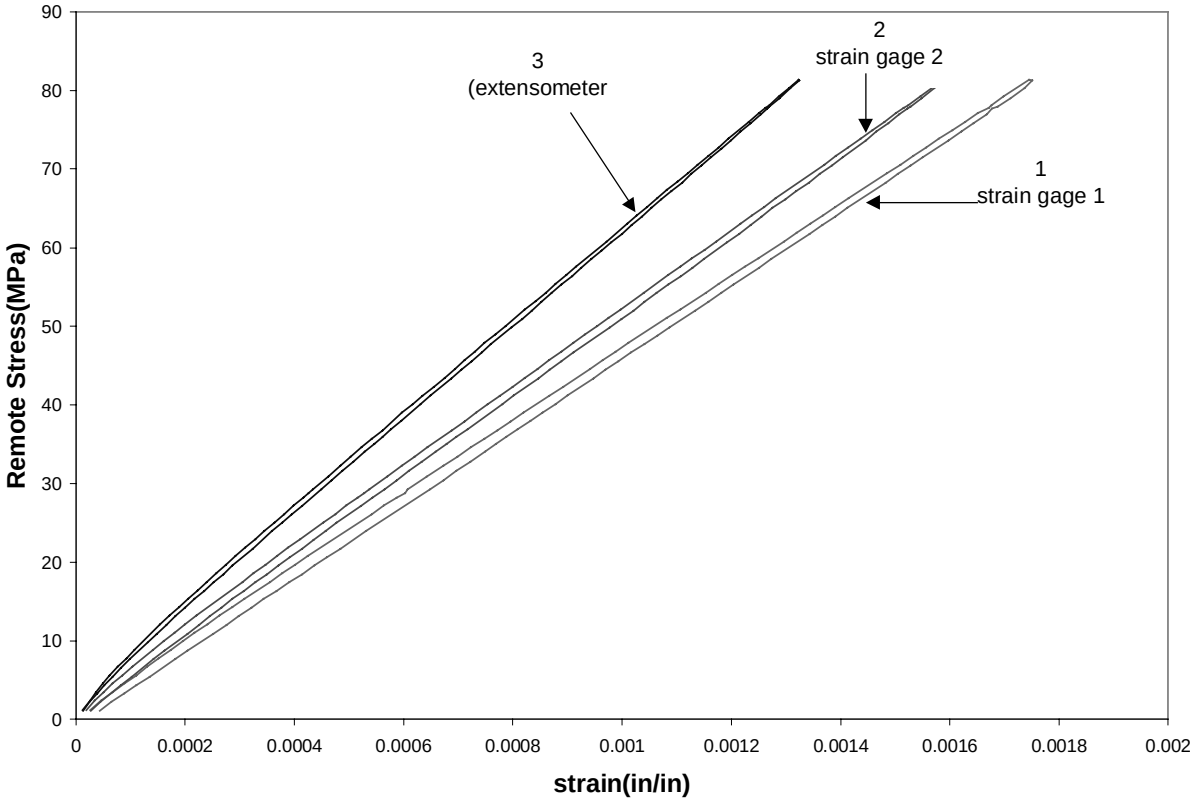

Figure 5.2 – Stress- strain plots at three different points in the notch specimen. Curve labeled 1 is the strain measured by strain gage 1(near the notch). Curve labeled 2 is the strain measured by strain gage 2(farther from the notch). Curve labeled 3 is the strain measured by the extensometer encompassing the notch.

A finite element model of the specimen geometry was developed to predict the stress-strain response. A quarter model was made and symmetric boundary conditions were applied at the two edges. Figure 5.3 shows the model geometry and the applied boundary conditions. The user –subroutine discussed in the previous chapter was used to input the material properties and the constitutive model. The stress-strain values from the analysis were compared to the experimental data. Two curves were plotted, one from the element just near the tip of the notch and the other far from the notch. Figure 5.4 shows the two curves as compared with the experimental data. The two curves show the extremes of the stress-strain behavior from the finite element analysis. The experimental data lie in between the two curves, which is an expected result. This is because the measurements were taken over a finite width rather than at a point and hence, the data represents average values over a given length. The finite element analysis gives a much larger amount of residual strain upon unloading and this is because the residual strain(ε_{in}) used to define the unloading modulus is dependent upon the maximum strain during loading. Hence, as the strain during loading increases, the permanent residual strain upon unloading also increases. This fact is supported by experimental data at low stresses but at high stresses the permanent strain upon unloading approaches a constant value rather than linearly increasing with strain. Also, the experiment was done at room temperature whereas the data used in the finite element model is based on the tests done at 1200 °C. Hence, the effect of temperature on the material properties is not taken into account in this model.

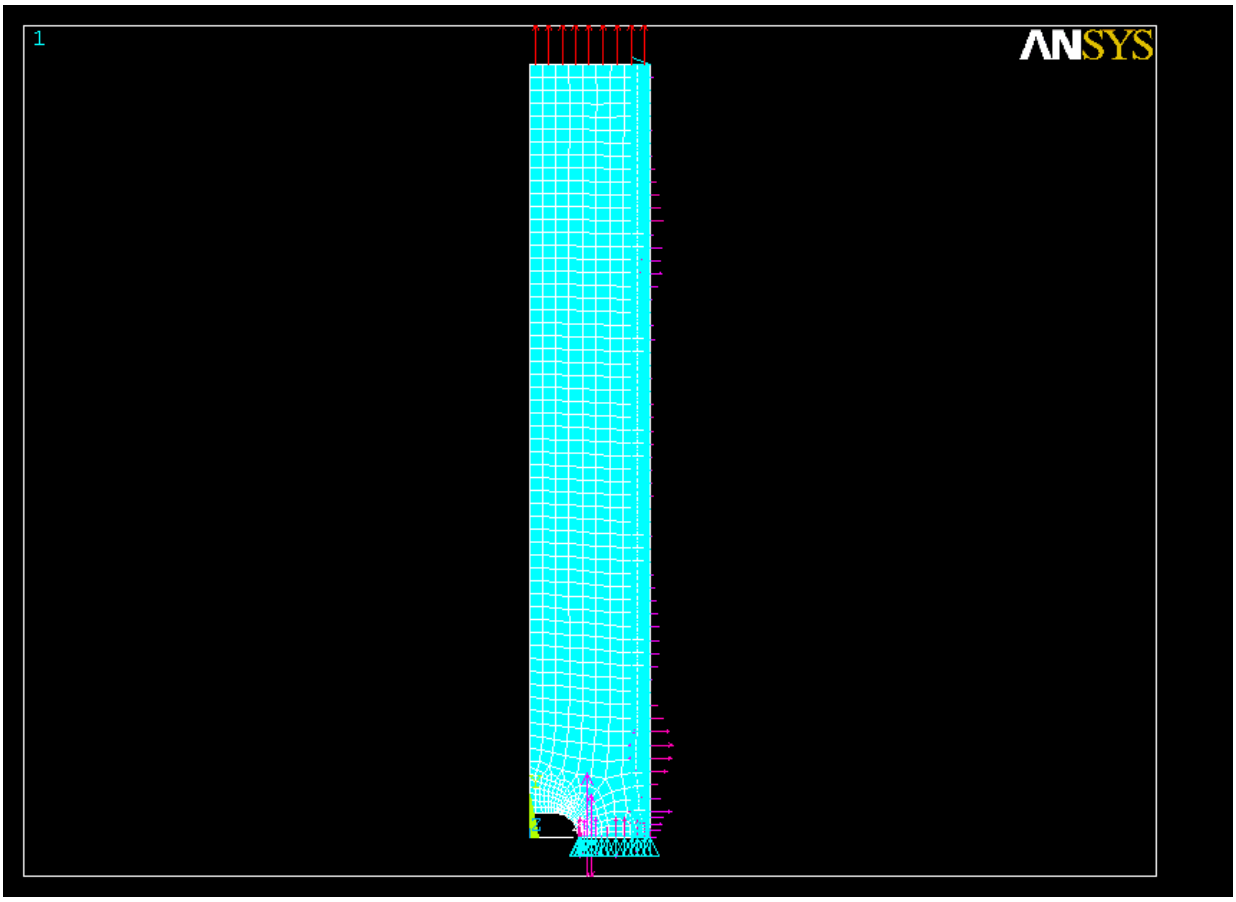

Figure 5.3 – The mesh and boundary conditions for the notched specimen geometry. This is a quarter model of the original geometry.

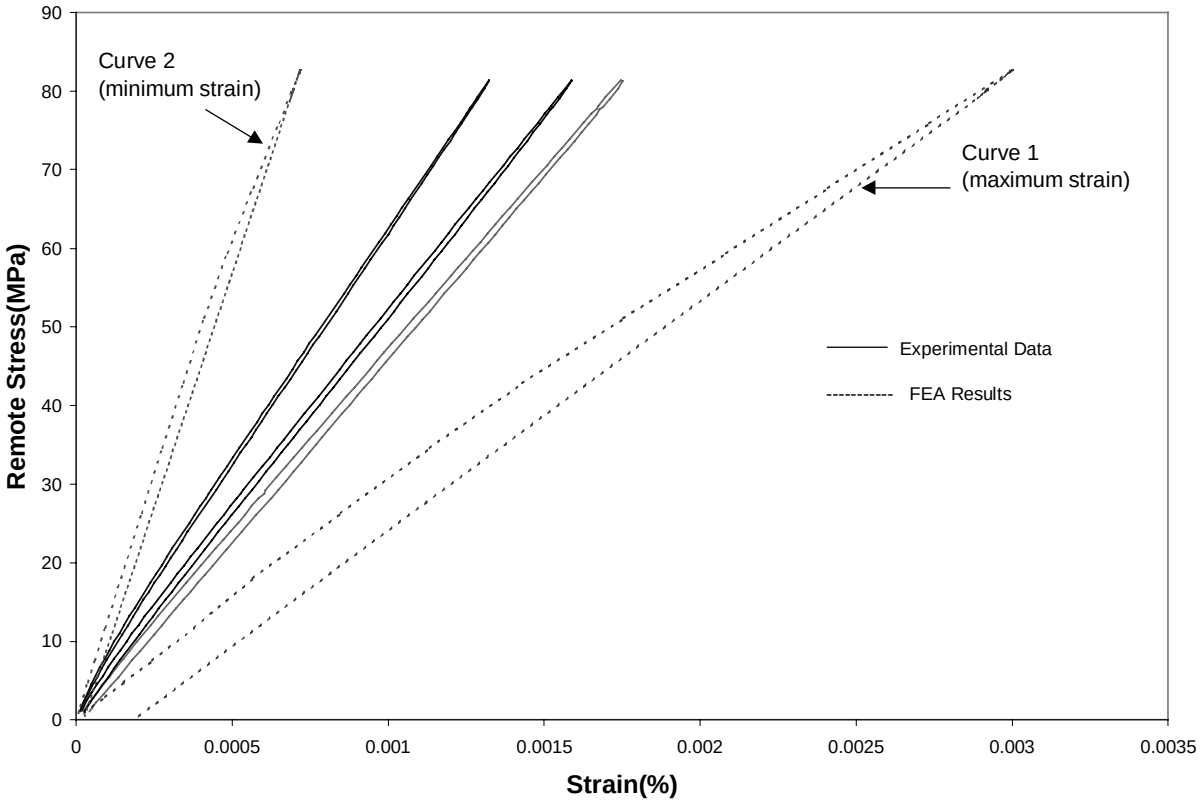

Figure 5.4 – Comparison of the experimental data with the Finite element analysis results. Curve 1 is the stress-strain plot for an element at the notch tip. Curve 2 is the stress-strain plot for an element far away from the notch.

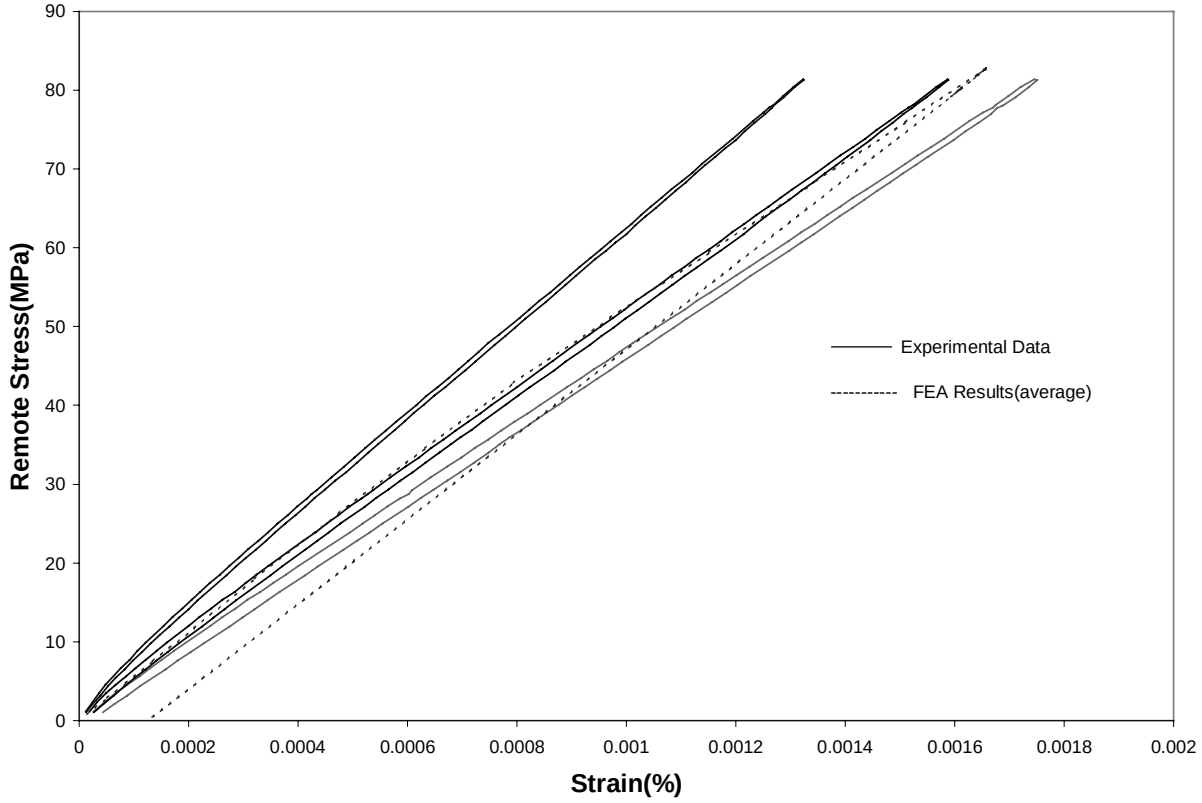

Figure 5.5 – Comparison of the experimental data with the average stress-strain curve. The dotted curve is obtained by averaging the stress-strain values over a distance equal to the width of the strain gage.

CHAPTER SIX

6.0. CONCLUSIONS

An empirical equation based on the test data was developed to express a relationship between creep strain and time, temperature and stress. The form of this equation is such that it can incorporate the pest behavior of CMC's at intermediate temperatures. At very low and very high temperatures, the equation reduces to a form similar to the Arrhenius rate equation. However, extrapolation based on the empirical equation is not recommended. The empirical equation was used as a constitutive equation in the finite element model. The results agreed with the experimental data and were as good or better than the time and strain hardening rules for creep analysis. The steady state strain rate shows dependence on temperature as well as stress. Hence, the Monkman-Grant equation was modified to include the effects of temperature on the strain rate. SiC/SiC composites exhibit non-linear behavior at high temperatures as shown by the quasi-static and creep tests and also supported by the microscopic examinations. The stress-strain behavior was not found to depend on temperature. The cyclic tests show the hysterisis type of stress-strain curves with the presence of a small amount of inelastic strain upon completely unloading. Also, at high temperatures, the material shows no hardening behavior. The non-linear material models such as plasticity or non-linear elasticity cannot be used to predict the unloading behavior of these materials. Hence, to model such material behavior, the bilinear kinematic hardening plasticity rule has to be modified. The unloading modulus is dependent on the maximum stress and strain during loading and hence, these quantities were used as state(or internal) variables. The results from the finite element analysis were compared with the

experimental data and they showed good agreement. The change in modulus with the number of cycles was also incorporated into the user subroutine and the results match closely with the experimental data. The same model was then used to predict the stress-strain behavior of a notched specimen. A test was done at room temperature to determine the behavior of notched specimens and the test provided some qualitative data about the notched response of the material. The data showed satisfactory agreement with the results from the finite element analysis. There is not enough data at present to model the dependence of the material properties on temperature. The model was developed assuming the material to be isotropic but it can be extended to anisotropic materials using concepts from anisotropic plasticity. Also, in the case of multi-axial state of stress, the unloading modulus can be calculated using an equivalent stress and strain. Though the modified plasticity model can correctly predict the unloading behavior, it fails to account for the recovery that occurs at high temperature. During loading the matrix cracks first and then the fibers take up all the load and when unloading takes place, the fibers unload but the matrix cracks are still there leading to a small permanent strain. At high temperatures, there is enough energy to close the matrix cracks leading to complete recovery. Hence, the phenomenon of recovery is temperature dependent.

7.0. REFERENCES

1. Pastor Michael S., Case Scott W and Reifsnider Ken L., January 1998, "Durability of Ceramic Matrix Composites", Quarterly Report.
2. Evans A. G., Zok F. W., McMeeking R. M., Du Z.Z., "Models of high-temperature assisted embrittlement in ceramic-matrix composites," *Journal of the American Ceramic Society*, v 79 n 9 Sept 1996, pp. 2345-2352.
3. Zok Frank W. and Steyer Todd E. A., December 1998, "Stress Rupture of an Enhanced Nicalon/Silicon Carbide Composite at Intermediate Temperatures," *Journal of the American Ceramic Society*, v 81 n 8 Aug 1998, pp. 2140-2146.
4. Karnitz Michael A., Craig Douglas F. and Richlen Scott L., " Continuous Fiber Ceramic Composite Program," *American Ceramic Society Bulletin* (70) 1991 pp. 430-435.
5. Miriyala Narendranath and Price Jefferey, Solar Turbines Inc., "CFCC News", No. 11, Fall 1999.
6. http://www.dlcomposites.com , Honeywell Advanced Composites Inc.
7. Naslain, R., "The concept of layered interfaces in SiC/SiC," *High Temperature Ceramic matrix composites II, Ceramic Transactions*, Vol. 58, pp. 23-40.
8. Besmann, T. M.,"CVI Processing of Ceramic Matrix Composites," *High Temperature Ceramic matrix composites II, Ceramic Transactions*, Vol. 58, pp. 1-22.
9. Heredia F.E., Mcnulty J. C.,Zok F. W., Evans A. G., "Oxidation embrittlement probe for ceramic-matrix composites," *Journal of the American Ceramic Society*, Vol 78(8), Aug. 1995, pp. 2097-2100.

10. Cao H.C., Bischoff E., Sbaizero O., Ruhle M., Evans A.G., Marshall D.B. and Brennan J.J., "Effect of Interfaces on the Properties of Fiber Reinforced Ceramics," *Journal of the American Ceramic Society*, Vol., 73, No. 6, 1990,pp. 1691-99

11. Zhu Shijie, Mizuno Mineo, Nagano Yasuno, Kagawa Yutaka and Kaya Hiroshi, " Creep and Fatigue Behavior in an Enhanced SiC/SiC Composite at High Temperature, " *Journal of American Ceramic Society*, Vol, 81, No. 9,1998, pp. 2269-2277.

12. Cao Jian-Wu, Mizuno Mineo, Nagano Yasuno., "The Stress Dependence Damage Mechanism during tensile creep and fatigue in a SiC/SiC composite at 1400 C," *Ceramic Engineering and Science Proceedings*, 19-3,1998,pp. 251-258.

13. Effinger Michael R., Tucker Dennis S., Barnett Teryy R., "Tensile and inter-laminar shear evaluation of Du Pont Lanxide CMCs," *Ceramic Engineering and Science Proceedings*, 17-4,1996,pp. 316-323.

14. Hebsur M. G., "Development and characterization of SiC(f)/MoSi3N4(p) hybrid composites, " *Material Science and Engineering A-structural materials properties microstructure and processing*, Vol. 261(1-2), March 15 1999, pp. 24-37.

15. Evans A. G., "Surface Ceramics and ceramic composites as high-temperature structural materials- challenges and opportunities, " *Phil. Trans. of the Royal Soc. Lond. Series A- Math. Phy. and Engg. Sci.*, Vol. 351(1697) Jun 15 1995, pp. 511-527.

16. Fox Dennis S., Nguyen N. Quyunhgiao, "Oxidation Kinetics of Enhanced SiC/SiC," *Ceramic Engineering and Science Proceedings*, 16-5,Sept-Oct 1998,pp. 877-844.

17. Mizuno Mineo, Zhu Shijie, Kagawa Yutaka, Kaya Hiroshi, "Stress, strain and elastic modulus behavior of SiC-fiber/SiC Composites during Creep and cyclic fatigue tests, " *Key Engineering Materials*, v 132-136 n Pt 3 1997 pp. 1941-1945

18. Lara Curzio E., "Stress-Rupture of Nicalon/SiC Continuous Fiber Ceramic Composites in air at 950 °C," *Journal of the American Ceramic Society*, v 80 n 12 Dec 1997, pp. 3268-3272.

19. Naslian R. R., “Processing of ceramic matrix composites,” *High Temperature Ceramic Matrix Composites III*, 164-1, 3-8, 1999.

20. Suemitsu et. al., “Improvement on the performance of ceramic gas turbine components by chemical vapor infiltration,” *Journal of the Japan Institute of metals*, 63(8), Aug. 1999, pp. 994-1001.

21. Penny R. K. and Mariott D.L., *Design for creep* , 2nd Edition , Chapman and Hall, 1995

22. Elahi Mehran, “ *Fatigue behavior of Ceramic Matrix Composites at elevated temperatures under cyclic loading,* “ PhD Thesis, Engineering Science and Mechanics, Virginia Polytechnic Institute and State University, 1996.

23. Dorn J.E. (1955) “Some Fundamental experimentson high temperature creep,” *J. Mech. Phys. Solids*. 3.

24. Garofalo F. (1965), *Fundamentals of Creep and Creep Rupture in Metals*, MacMillan, New York

25. Zhu S., Mizuno M., Kagawa Y. and Ochi Y., “Creep Deformation and fracture of SiC/SiC composites,” *Key Engineering Materials*, Vols. 171-174, 2000 pp. 755-762.

26. Monkman F.C. and Grant N.J., *Proc. Am. Soc. Test. Mater*., 56(1956) p. 593

27. Larson F.R. and Miller J., *Trans. ASME,* 74(1952), p. 765

28. Verrilli M.J., Calomino A.M. and Brewer D.N., “Creep-rupture behavior of a Nicalon/SiC composite,” *Thermal and Mechanical Test Methods and Behavior of Continuous-Fiber Ceramic Composites*, ASTM, 1997

29. Robatonov Y.M., Some problems on the theory of creep, *NACA TM 1353*, 1953

30. Boyle J.T. and Spence J., *Stress Analysis for Creep*, Butterworth & Co., 1983 pp.162-167.

31. Zienkiewicz O.C. and Taylor R.L., *The Finite Element Method*, Vol. 2, Dynamics and non-linearity, McGraw Hill,1991

32. Naslain R.R., “Processing of Ceramic Matrix Composites,” *Key Engineering Materials*, Vols. 164-165(1999) pp. 3-8

33. Holmes J.W., Park Y.H., “Finite element modeling of creep deformation in fiber reinforced ceramic composites,” *Journal of Material Science*, 27,1992,pp 6341-6351

34. Chermant J.L. and Holmes J., “Elevated temperature creep and cyclic creep behavior of fiber reinforced ceramics,” *Journal of the American Ceramic Society*

35. Holmes J.W., Park Y.H., Jones J.W., “ Tensile creep and creep recovery behavior of a SiC fiber-Si_3N_4 composite,” *Journal of the American Ceramic Society*,76[5],1281-1293,1993

36. Zhu S., Mizuno M., Nagano Y., Kagawa Y and Kaya H., " Tensile creep behavior of a SiC-fiber/SiC composite at elevated temperatures," *Composites Science and Technology*, Vol. 57, 1997, 1629-1637.

37. Ferber M. and Jenkins M., "Evaluation of the strength and creep-fatigue behavior of hot isostatically pressed silicon nitride," *Journal of the American Ceramic Society*, Vol. 75, pp. 2453-2462.

38. Leucke W., Wiederhorn S., Hockey B., Long G., "Cavity Evolution during tensile creep of Si3N4," *Materials Research Society Symposium Proceedings*, vol 287, pp. 467-472.

39. Menon M., Fang H., Wu D., Jenkins M. and Ferber M., "Creep and stress rupture of an advanced silicon nitride: Part III, Stress Rupture and Monkman-Grant Relationship, "*Journal of the American Ceramic Society*, vol. 77, pp. 1235-1241.

40. Powers L.M., Jadaan O.M., Gyekenyesi J.P., "Creep life of ceramic components using a finite element based integrated design program(CARES/CREEP)," *ASME 96-GT-369*.

41. *ANSYS Theory Reference*, 000855, Eight Edition, Version 5.4.

42. Burr A, Hild F, Leckie FA," On the mechanical behavior under cyclic loading of ceramic matrix composites", *Materials Science and Engineering A-Structural Materials Properties Microstructure and Processing***,** 250: (2) 256-263 Jul 31 1998

43. *Monotonic Tensile Testing of Ceramic Matrix, Intermetallic Matrix and Metal Matrix Composite Materials*, HSR/EPM-D-001-93 Consensus Standard, GE Aircraft Engines, 1 Neumann Way, Mail Drop G-50, Cincinnati, OH, 45215-6309

8.0 VITA

Vinayak Pandey received his Bachelor's Degree (1997) in Mechanical Engineering from The Institute of Technology, Banaras Hindu University, Varanasi, India. He joined the Tata Engineering and Locomotive Company Ltd., India as a graduate engineer trainee for a short period, before joining Case Western Reserve University, to pursue his Master's Degree in mechanical Engineering. After a year, he transferred to Virginia Tech. to pursue his master's degree in Engineering Science and Mechanics. At Virginia Tech., he worked on studying the high temperature behavior of ceramic matrix composites. After his graduation from Virginia Tech., he will be working as a Mechanical Design Engineer, in the Advanced Technology Development division at Intel Corporation.